Kinetics and reactor modelling of a complex three-phase system: Carbonation of epoxides on grafted catalysts

Tapio Salmi, Wander Perez-Sena, Fabrizio Ciccarelli, Kari Eränen, Ananias Medina, Tommaso Cogliano, Martino Di Serio, Johan Wärnå, Sébastien Leveneur, Vincenzo Russo

Chemical Engineering Science 285 (2024) 119578

Contents lists available at ScienceDirect

Chemical Engineering Science

journal homepage: www.elsevier.com/locate/ces

Kinetics and reactor modelling of a complex three-phase system: Carbonation of epoxides on grafted catalysts

Tapio Salmi [a], Wander Y. Perez-Sena [a,b], Fabrizio Ciccarelli [c], Kari Eränen [a], Ananias Medina [a], Tommaso Cogliano [a,c], Martino Di Serio [c], Johan Wärnå [a], Sébastien Leveneur [a,b], Vincenzo Russo [a,c]

[a] Åbo Akademi University, Laboratory of Industrial Chemistry and Reaction Engineering (TKR), FI-20500 Turku/Åbo, Finland
[b] Normandie Université, INSA Rouen, Laboratoire de Sécurité des Procédés Chimiques (LSPC), FR-76000 Rouen, France
[c] Università di Napoli Federico II, Chemical Sciences Department, IT-80126 Napoli, Italy

ARTICLE INFO

Keywords:
Carbonation
Cycloaddition
Fatty acid
Carbon dioxide
Grafted catalyst
Kinetics
Three-phase reactor
Mathematical modelling

ABSTRACT

Fatty acid epoxides are obtained by epoxidation of fatty acids and esters with hydrogen peroxide. Carbonation of fatty acid epoxides with CO_2 is an important topic in the development of environmentally friendly technologies for the production of chemical intermediates, polymers and fuel components. Very precise kinetic and mass transfer studies on the carbonation of a tall-oil model component, epoxidized methyl oleate were carried out in an autoclave operating at 20–60 bar CO_2 and 100–160 °C. SBA-15(0.12)-4PPI was used as the grafted heterogeneous catalyst. The reaction times were 0–23 h and the stirring rates were varied between 200 and 1000 rpm to study the gas–liquid mass transfer of CO_2. The main reaction product was the carbonate, while some amounts of ketone were formed as a side product via the Meinwald rearrangement. Five rival reaction mechanisms were considered, based on the concept of interaction between the Lewis and nucleophilic sites on the catalyst surface. A multiphase reactor model including the interaction of intrinsic kinetics and gas–liquid mass transfer effects was developed to determine the parameters from the experimental data. The model reproduced the experimental data very well, giving a perspective for process scale-up.

1. Introduction

Cyclic carbonates are used as polymer precursors, fuel additives and solvents (Saptal and Bhanage, 2017). Cyclic carbonates provide an environmentally friendly and non-toxic pathway to the production of polyurethanes, which are unfortunately still made from polyols and di-isocyanates (Kreye et al., 2013; Petrović, 2008; Saptal and Bhanage, 2017). The currently applied isocyanate based synthesis route involves the use of the very toxic compound, phosgene (LC_{50} 500 ppm, human, 1 min) (National Center for Biotechnology Information, 2023) so the need for a new and green technology is urgent. It is well known that cyclo-addition of carbon dioxide to epoxides in the presence of homogeneous and heterogeneous catalysts gives cyclic carbonates (Webster, 2003). The entire process can be sketched as follows,

Unsaturated fatty acid → Epoxide → Carbonate → Polymer

Epoxides can be obtained from the reaction between unsaturated fatty acid or fatty acid ester with hydrogen peroxide (Alves et al., 2015). Several technologies exist for the epoxidation of unsaturated fatty acids, such as the classical indirect process discovered originally by Prilezhaev in the presence or absence of an added acid catalyst (e.g. mineral acid, acidic ion exchange resin) as well as direct enzymatic and heterogeneously catalyzed process (Freites Aguilera et al., 2020; Vanags et al., 2023; Wikström et al., 2023).

Unsaturated fatty acids and their esters are found in several edible and non-edible oils, such as soybean, palm, rapeseed, linseed, corn, sunflower, cardoon, castor, jathropha, cottonseed, grapeseed and canola oils and they are reactive in epoxidation with hydrogen peroxide. In the Northern hemisphere, the epoxides obtained from tall oil fatty acids are of particular interest, because large amounts of non-edible tall oil are obtainable as side streams from the Kraft pulping process, i.e. from cellulose production Studies concerning the epoxidation of vegetable oils were mainly performed using first generation biomass. Fortunately, in the last decade, the trend has changed, focusing mainly on either second or third generation biomass as the raw material. The dominant chemical compounds in tall oil are oleic (48 %) and linoleic (35 %) acids. All these acids and their esters contain double bonds, which in principle can be epoxidized either by using the classical Prilezhaev concept, heterogeneous catalysts or enzymatic technology. For instance, Freites Aguilera et al. (2020) studied both tall oil fatty acids and distilled tall oil in the epoxidation reaction via the Prilezhaev concept. Amberlite IR120 and other acidic ion exchange resins (AIERs) were used as heterogeneous acid catalysts and the traditional semibatch reactor configuration was compared with an improved loop reactor configuration by the use of

https://doi.org/10.1016/j.ces.2023.119578
Received 25 September 2023; Received in revised form 21 November 2023; Accepted 28 November 2023
Available online 9 December 2023

Nomenclature

A	gas–liquid interfacial area
A, B	parameters in cubic equation of state
a,b	parameters in Peng-Robinson equation of state
a_L	gas–liquid interfacial area-to-liquid volume ratio
a_G	gas–liquid interfacial area-to-gas volume ratio
c	concentration
K	equilibrium constant
k	rate constant
k_L	liquid-phase mass transfer coefficient
m	mass
N	diffusion flux
n	amount of substance
n	flow of amount of substance (molar flow)
P	pressure
Q	objective function in regression analysis
R	reaction rate
R^2	degree of explanation
R_G	general gas constant, 8.314 J/(Kmol)
r	rate
T	temperature
t	time
V	volume
y	dimensionless epoxide concentration
Z	compressibility factor
z	transformed variable
α, α'	merged parameters
β, β'	merged rate parameter
γ	merged kinetic parameter
δ	dimensionless adsorption parameter
κ	dimensionless adsorption parameter
λ	merged parameter
ρ	density
ω, ω'	combined adsorption and rate parameters

Subscripts and superscripts

B	bulk quantity
cat	catalyst
exp	experimental quantity
G	gas phase
i	component index
L	liquid phase
t	time
0	initial value or total amount
*	surface site, saturation state

Abbreviations

C	carbon dioxide
E	epoxide
CMO	carbonated methyl oleate
EMO	epoxidized methyl oleate
EoS	equation of state
IVP	initial value problem
ODE	ordinary differential equation
P1	product 1, epoxide
P2	product 2, ketone
PR	Peng-Robinson
MCMC	Markov Chain Monte Carlo
TEOS	tetraethyl orthosilicate

microwave irradiation. It was noticed that the physicochemical properties of the distilled tall oil, such as the higher amount of rosin acids and the higher viscosity, had promoted the ring opening reactions and limited the interfacial mass transfer, resulting in lower yields of the reaction products. Wikström et al. (2023) investigated the tall oil fatty acid epoxidation in the presence of *Candida Antartica* B lipase immobilized on Novozym 435 in batch and semibatch reactor configurations. Vanags et al. (2023) studied the chemo-enzymatic epoxidation of tall oil fatty acids in the presence of six different lipase enzymes. *Antartica* lipase B immobilized on Novozym 435 performed better than all the other unsupported lipases. The reaction system was also studied in a continuous reactor configuration, where a continuous stirred thank reactor was connected to a tubular reactor equipped with several layers of a solid catalyst, namely *Antartica* lipase B immobilized on Novozym 435. Despite the results in the batch configuration gave good results under solvent-free conditions, so in the continuous configuration the presence of a solvent, toluene, improved the performance by decreasing the viscosity of the reaction mixture. From the viewpoint of process engineering, esters of fatty acids are favorable epoxidation reagents, because they have lower viscosity than the fatty acid itself and its epoxidation products (Cai et al., 2019; Pérez-Sena et al., 2021).

On paper, carbonization of an epoxide is a straightforward process – the epoxide reacts in the liquid phase with dissolved carbon dioxide – but the reaction rate and the product selectivity are still the major challenges. The carbonation, the cycloaddition reaction between the epoxide and carbon dioxide leading to the carbonated product requires the presence of a catalyst. Several homogeneous and heterogeneous catalysts have been screened and the cycloaddition kinetics and product selectivities have varied a lot, depending on the catalyst and the reaction conditions (Decortes et al., 2010; Lu and Darensbourg, 2012; Honda et al., 2014; Luo et al., 2014; Su et al., 2014; Alves et al., 2015; Comerford et al., 2015; Kohrt and Werner, 2015; Sankar et al., 2015; Huang et al., 2016; Liu et al., 2016; Zhang et al., 2016; Liang et al., 2018; Longwitz et al., 2018; Zhao et al., 2019; Hu et al., 2020). Extensive reviews on various carbonation catalysts have been provided by North et al. (2010) and Calabrese et al. (2019). Compared to smaller molecules, the carbonation of fatty acid epoxidesis more demanding, because the larger molecule size as such implies a suppressed reactivity and an increasing steric hindrance. However, high efficiency and carbonate selectivity has been reported, e.g. for fatty acid carbonation in the presence of a homogeneous al complex (Pena Carrodeguas et al., 2017).

The use of heterogeneous catalysts instead of homogeneous ones has a great advantage from the viewpoint of process engineering: the separation of solid heterogeneous catalysts from the reaction mixture is straightforward compared to the separation and recycling of homogeneous catalysts. Two main trends are visible in the contemporary literature: heterogenization of efficient and selective homogeneous catalysts or direct use of a heterogeneous catalyst. Examples of heterogenization are organocatalysts on silica gel (Kohrt and Werner, 2015), and ionic liquid based catalysts on solid supports (Sankar et al., 2015; Zhang et al., 2016). Particularly graphene oxide has been successfully used as a solid matrix for heterogenization (Zhang et al., 2016). Several heterogeneous catalysts have been screened, for instance cobalt (Lu and Darensbourg, 2012), zinc (Luo et al., 2014), magnesium and cerium oxides (Zhao et al., 2019; Honda et al., 2014), LiBr/γ-Al_2O_3 (Liang et al., 2018) and graphitic carbon nitride (Su et al., 2014; Huang et al., 2016), but in general, the homogeneous catalysts have shown a better performance concerning the epoxide conversion. Heterogenization of active and selective homogeneous catalysts by grafting can provide a way to combine the benefits of homogeneous and heterogeneous catalysis; for example Bähr and Mülhaupt (2012) report the use of TBAB on silica for the epoxidation of soybean and linseed oils: a complete conversion of the epoxides was obtained within 20 h. TBAB was confirmed to be an active catalyst in the carbonation of castor oil, too (Ruiz et al., 2017). Motokura

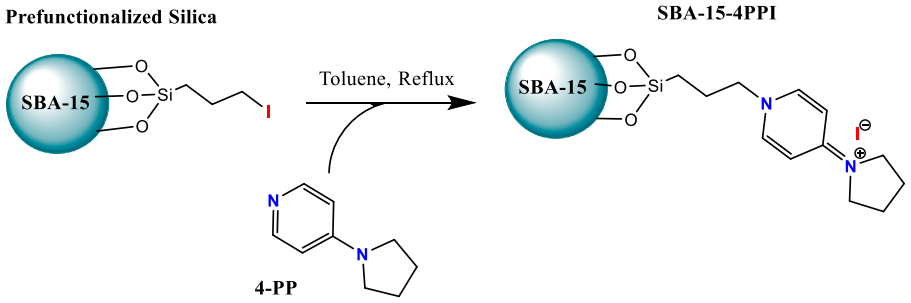

Fig. 1. Heterogenized cycloaddition catalysts prepared in our previous work (Perez Sena et al., 2022).

and co-workers (2009) used silica supported aminopyridium halides in the epoxidation of styrene oxide and high yields of cyclic carbonate were obtained for this kind of crafted catalyst. A characteristic feature for the previous carbonation studies is that very precise kinetic modelling is missing, even though excellent kinetic data have been obtained with a high precision and using the most sophisticated techniques, such as NMR and infrared spectroscopy.

In the previous work, we focused on the heterogenization of homogeneous catalysts for the carbonation process (Perez Sena et al., 2022). Several active species were successfully anchored to SiO_2 and SBA-15 as illustrated in Fig. 1. The catalysts were used in the carbonation of epoxidized methyl oleate (EMO) with carbon dioxide in an isothermal and pressurized reactor autoclave. In this article, we report new results on carbonation kinetics for the SBA-15 supported 4-pyrrolidinopyridinium (SBA-15-4PPI) catalyst. EMO was used the substrate and extensive kinetic and mass transfer experiments were conducted in a pressurized autoclave operating under isothermal conditions. Kinetic models based on presumed molecular mechanisms for the cycloaddition of carbon dioxide to epoxides are presented and the modelling results are discussed from the viewpoints of reaction mechanisms and reactor technology.

2. Experimental section

2.1. Materials and chemicals

The following chemicals were used in catalyst preparation and in kinetic experiments: tetraethyl orthosilicate (TEOS, ≥98 %), PEG-PPG-PEG (pluronic123), (3-iodopropyl)trimethoxysilane (≥95 %), 4-pyrrolidinopyridine (≥98 %), toluene (≥99.8 %), methanol (≥99.9 %), ethyl acetate (≥99.9 %), oleic acid (≥90 %), sulfuric acid (95–97 %), formic acid (≥98 %) were all purchased from Sigma Aldrich. Hydrogen peroxide solution (≥30 %) were provided by Fisher Scientific, zinc nitrate (≥99 %) by Fluka and dichloromethane (DCM) (≥99.9 %) by Honeywell. Carbon dioxide (99.995 %) was obtained from Woikoski Oy. The commercial materials and chemicals were used as received. The methyl ester of oleic acid was prepared in laboratory from oleic acid and methanol in the presence of sulfuric acid as the homogeneous catalyst. The methyl ester was epoxidized with hydrogen peroxide according to the Prilezhaev concept. Formic acid was used as the reaction carrier in the epoxidation. The synthesis was carried out in semibatch mode by adding gradually hydrogen peroxide to the reaction mixture. The preparation of the methyl ester and its epoxide followed exactly the procedures given in our previous publications (Perez Sena et al., 2022; Guzmán Agudelo et al., 2020).

2.2. Catalyst preparation

The catalytic material used in the carbonation experiments was prepared following a well-established multi-step synthesis procedures described below. The solid mesoporous material was prepared and pre-functionalized, after which the active catalyst component was grafted to it.

2.2.1. SBA-15 synthesis

The SBA-15 mesoporous material was prepared as follows: 2 g of PEG-PPG-PEG copolymer were dissolved in 75 mL of 1.6 M HCl solution for 4 h at 40 °C. Once a completed dissolution was achieved, 4.0 g of TEOS were gradually added to the solution. Thereafter, the solution was maintained under vigorous stirring at 40 °C for 24 h. The resultant mixture was transferred into a Teflon liner and kept under static condition at 100 °C for additional 24 h. Following this, the mixture was filtered, yielding a white solid. This solid material was then subjected to calcination at 550 °C, employing a heating rate of 1 °C min^{-1}, for a total period of 6 h. The obtained SBA-15 material was stored in a desiccator, ensuring optimal conditions for future functionalization.

2.2.2. Iodine pre-functionalization of SBA-15

The previously synthesized SBA-15 (10.0 g) was dispersed in a 500 mL toluene solution containing 3-iodopropyltrimethoxysilane (50.0 mmol). The resulting solution was subjected to refluxing under an inert atmosphere for 24 h. After this reflux, the mixture was allowed to cool, and the solid material was recovered by filtration. The solid was washed three times with fresh toluene, followed by washing with ethanol in a Soxhlet extractor for 24 h, ensuring a complete removal of free species from the surface. After the purification steps, the solid material was subjected to drying at 70 °C overnight. The dried material was stored appropriately for future functionalization.

2.2.3. Preparation of SBA-15 supported 4-pyrrolidinopyridinium (SBA-15-4PPI)

The synthesis of the catalytic material SBA-15-4PPI was conducted as follows. Initially, Iodine pre-functionalized SBA-15 (10.0 g) and 4-pyrrolidinopyridinium (60.0 mmol) were combined in a toluene solution (500 mL). This mixture was subjected to reflux conditions under an inert atmosphere for 24 h. Following this period, the mixture was cooled down, and the resulting solid was collected by filtration. Thereafter, the solid was washed three times with toluene, water and dichloromethane, followed by an additional wash with ethanol in a Soxhlet extractor for 24 h. The catalytic material was dried overnight at 70 °C and appropriately stored for future use.

2.3. Carbonation experiments

Kinetic and mass transfer experiments were carried out in a 300 mL autoclave reactor equipped with mechanical stirring. In typical carbonation experiment, 50 g of epoxidized methyl oleate and 4 g of the synthesized SBA-15-4PPI catalyst were mixed in the reactor vessel. The reactor was sealed and purged with nitrogen three times. Thereafter, the reaction mixture was heated to the target temperature, and once achieved, pure CO_2 was fed continuously into the system at a constant pressure. The reactor pressure was regulated by a pressure controller so

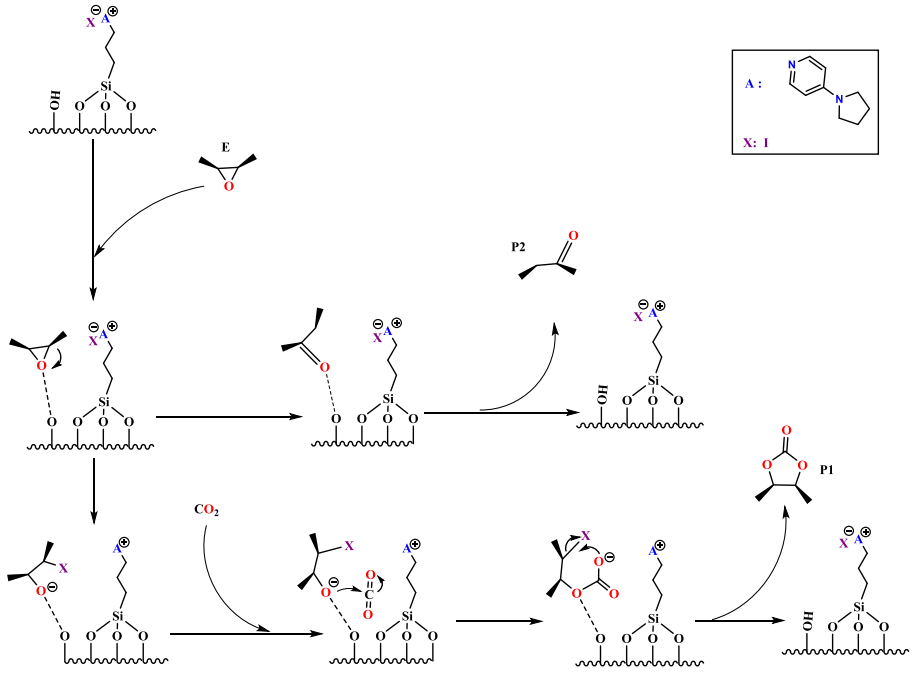

Mechanism 1

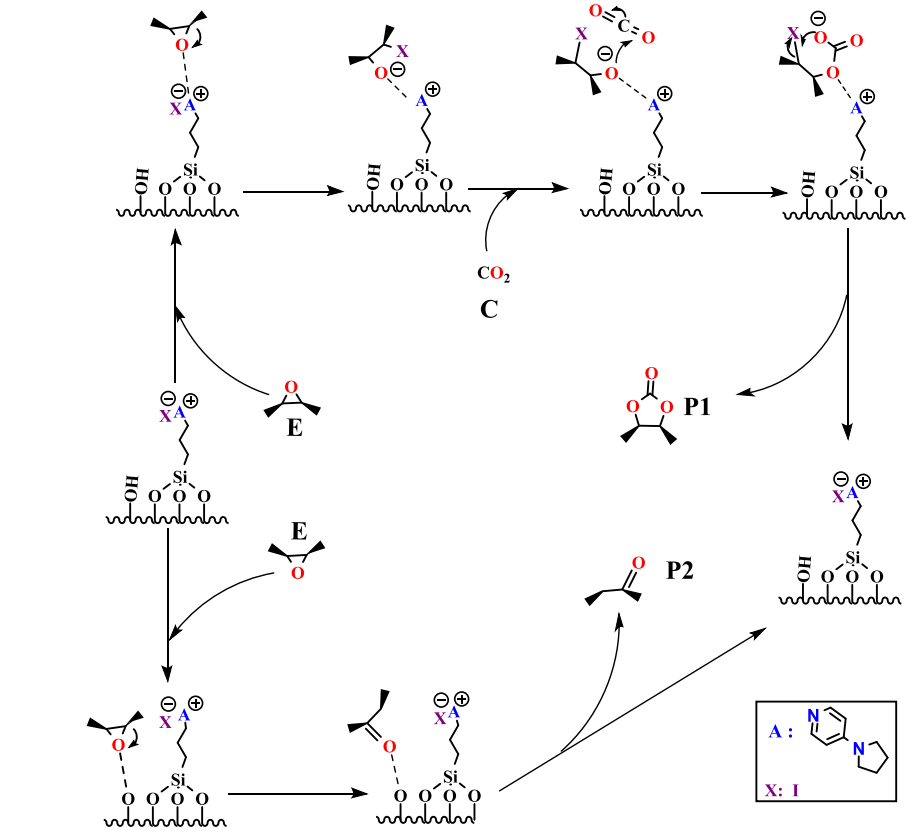

Mechanism 2

Fig. 2. Rival reaction mechanisms investigated in this work.

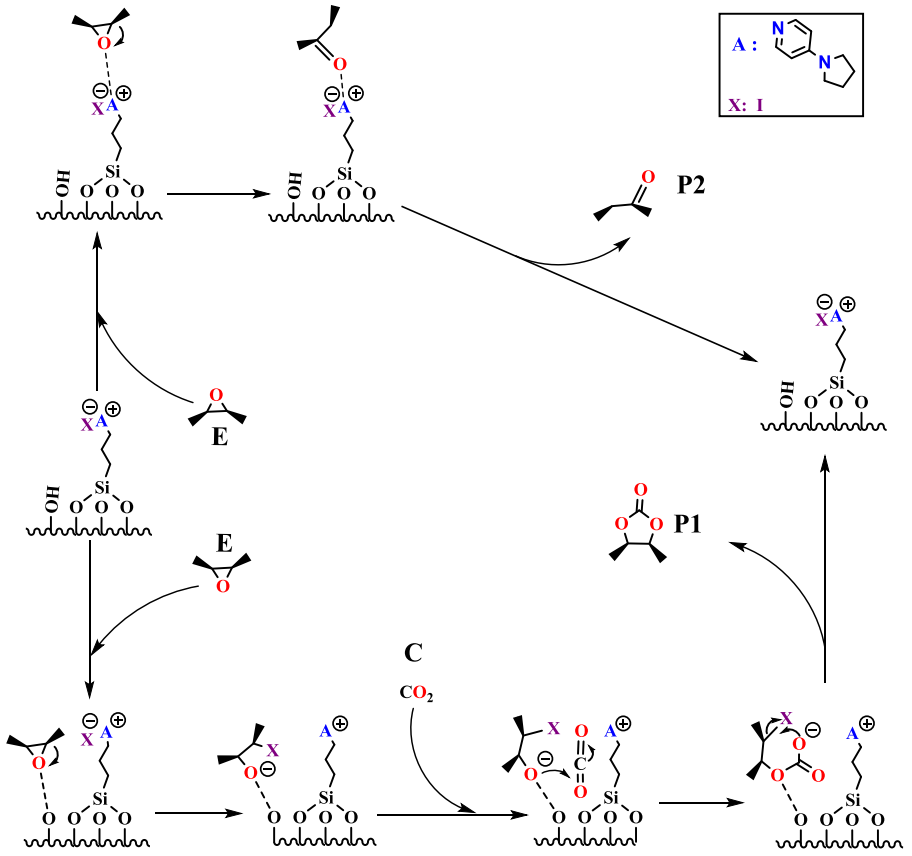

Mechanism 3

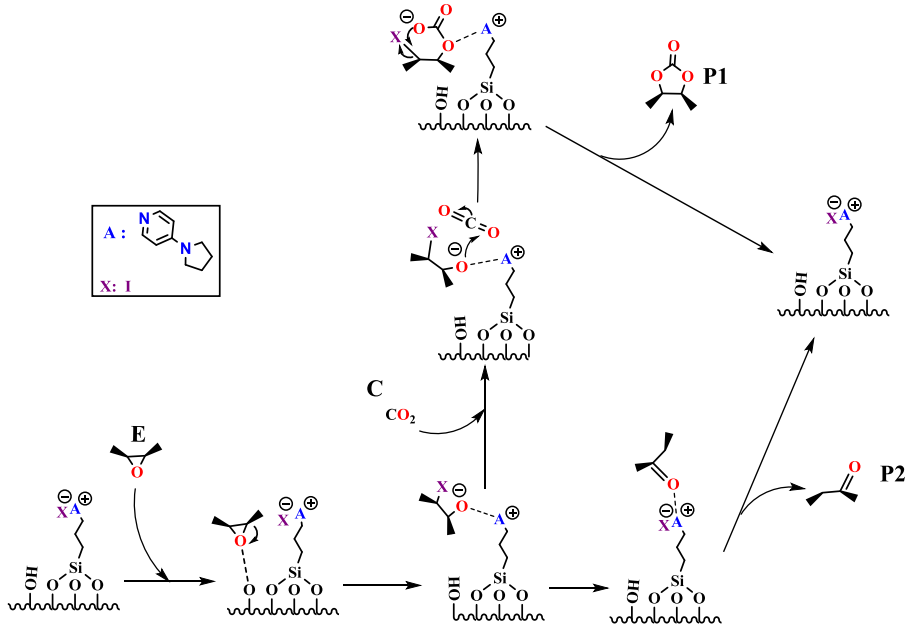

Mechanism 4

Fig. 2. (*continued*).

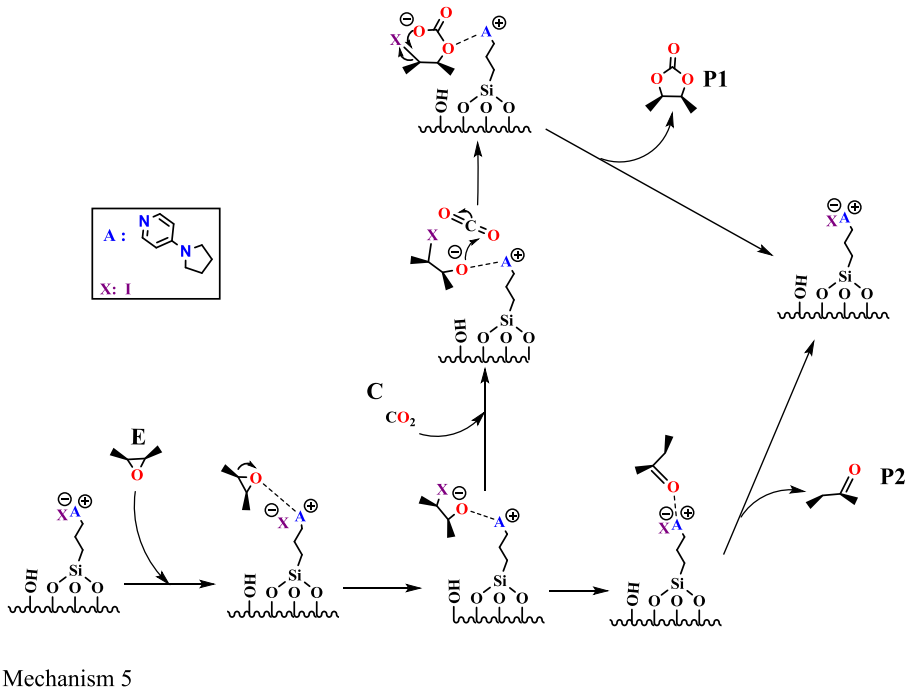

Mechanism 5

Fig. 2. (*continued*).

that the CO_2 pressure remained constant during the experiment. The pressure was monitored continuously and the pressure data were stored on a PC. To ensure excellent gas–liquid mixing, a gas-entrainment impeller was used at 800 rpm.

Samples were withdrawn periodically from the reactor to follow the progress of the reaction. The epoxide concentration was analyzed by the oxirane titration method of Jay (1964) following the standard ASTM D 1652-04, 2004. Perchloric acid is added to tetraethylammonium chloride (TEAB) to generate in situ hydrogen bromide, which titrates the epoxy groups in the stoichiometric ratio 1:1. The progress of titration was followed by a potentiometric titrator. The accuracy of the method was approx. 5 %. The carbonate concentration was measured using a combination of ^{1}H NMR and FTIR spectroscopy. The FTIR analysis was based on the carbonate group absorbance at 1800 cm^{-1} as described in our previous publications (Perez Sena et al., 2022; Guzmán Agudelo et al., 2020).

2.4. Gas-liquid mass transfer experiments

Gas-liquid mass transfer experiments were conducted in the same reactor vessel, which was utilized for the kinetic studies. Both the reactant (epoxidized methyl oleate, EMO) and the product (carbonated methyl oleate, CMO) were employed in these experiments.

In a typical mass transfer experiment, either epoxidized methyl oleate or carbonated methyl oleate was introduced into the reactor vessel and the reactor was sealed and purged several times with nitrogen before heating it to a predefined temperature under gentle stirring. Once a stable temperature was achieved, the stirring was switched off, and CO_2 was introduced until the desired pressure was reached in the reactor vessel. Then the feed was closed off, and the CO_2 transfer from the gas phase to the liquid phase was initiated by starting the mechanical stirring. The gas-phase pressure and temperature, and the liquid phase temperature were continuously recorded throughout during the experiment. The amount of CO_2 (in mol) transferring into the liquid phase was calculated from the decrease of the CO_2 concentration in the gas phase.

Prior to the mass transfer experiments, the total volume of the sealed reactor vessel was determined by interconnecting the empty reactor vessel to a reservoir of a known volume. The temperature and pressure of both the reservoir and the reactor vessel were monitored. The reservoir was initially filled with either CO_2 or N_2, and subsequently, the total amount of gas contained in the reservoir was distributed between the two vessels by adjusting a valve. The volume of the reactor was calculated by using a gas law. The Peng-Robinson equation of state (Reid et al., 1988) was used to estimate the compressibility factor of the employed gas during the determination of the reactor volume and during the mass transfer experiments.

3. Reaction mechanism and kinetic model

3.1. Overview of presumed reaction mechanisms

The main reaction, the carbonation of epoxidized fatty acid ester follows the stoichiometry

Epoxide + CO_2 → Carbonated product

The experimental data however revealed that besides the epoxidized product, a ketone was formed, according to the simple the stoichiometry

Epoxide → Ketone

The ketone formation was irreversible and essentially parallel with the epoxide formation. The crucial issue is the path of this side reaction, particularly on which active sites, the Lewis sites or the nucleophilic sites, are involved in this side reaction. Several possible pathways were considered, by detailed kinetic analysis of the experimental data and by separate experiments conducted in the absence of carbon dioxide. In total, five alternative reaction mechanisms were compared, as displayed in Fig. 2.

The essential features and basic hypotheses of the investigated mechanisms are summarized below.

Mechanism 1. Carbonation is initiated on the Lewis site, and adsorbed epoxide interacts with the nucleophilic site forming an intermediate, which reacts with dissolved CO_2 to the carbonated product, which desorbs from the surface. The ketone formation is presumed to take place on the Lewis site.

Mechanism 2. Carbonation takes place directly on the nucleophilic site, while the ketone formation proceeds on the Lewis site.

Mechanism 3. Carbonation proceeds similarly to mechanism 1, via the interaction of Lewis and nucleophilic sites, whereas the ketone is

Table 1
Elementary steps in mechanisms 1–5.

Mechanism 1 (*1 = Lewis site, *2 = nucleophilic site)	
1	E + *1 = E*1
2	E*1 + *2 → F*2 + *1
3	F*2 + C → P1*2
4	P1*2 = P1 + *2
5	E*1 → P2*1
6	P2*1 = P2 + *1
Mechanism 2	
1	E + *1 = E*1
2	E + *2 = E*2
3	E*2 + C → P1*2
4	P1*2 = P1 + *2
5	E*1 → P2*2
6	P2*2 = P2 + *2
Mechanism 3	
1	E + *1 = E*1
2	E + *2 = E*2
3	E*1 + *2 → F*2 + *1
4	F*2 + C → P1*2
5	P1*2 = P1 + *2
6	E*2 → P2*2
7	P2*2 = P2 + *2
Mechanism 4	
1	E + *1 = E*1
2	E*1 + *2 = F*2
3	F*2 + C → P1*2
4	P1*2 = P1 + *2
5	F*2 → P2*2
6	P2*2 = P2 + *2
Mechanism 5	
1	E + *2 = E*2
2	E*2 + C → P1*2
3	P1*2 = P1 + *2
4	E*2 → P2*2
5	P2*2 = P2 + *2

formed on the nucleophilic site.

Mechanism 4. The reaction is initiated on the Lewis site, the reaction intermediate is shifted to the nucleophilic site, where the carbonated product and the ketone are formed in parallel.

Mechanism 5. This mechanism is based on the single site concept, i.e. both the carbonization and the ketone formation take place in parallel on the nucleophilic site.

The common feature for these mechanisms is that the reactant (E = epoxide) and the product (P1 = carbonated product, P2 = ketone) adsorption is included, whereas CO_2 reacts from the bulk liquid. In this sense, the mechanisms follow the Eley-Rideal concept. The adsorption and desorption steps are presumed to be rapid compared to the surface reaction steps. Consequently, the quasi-equilibrium hypothesis is applied to the adsorption and desorption steps. For the surface intermediates, the quasi-steady state hypothesis is used, in order to reduce the number of adjustable parameters in the rate equations. The rate determining steps are regarded as irreversible. The elementary steps included in mechanisms 1–5 are summarized in Table 1.

3.2. Rate equations

Based on the mechanisms and the hypotheses presented above, we arrive at the following rate equations (R_I = carbonation rate, R_{II} = ketone formation rate); the details of the derivations are provided in Supplementary Information.

Mechanism 1

$$R_I = \frac{k_C C_E C_C}{1 + \alpha C_E + \beta C_E C_C + K_{P1} C_{P1} + K_{P2} C_{P2}} \quad (1)$$

$$R_{II} = \frac{k_K C_E}{1 + \alpha C_E + \beta C_E C_C + K_{P1} C_{P1} + K_{P2} C_{P2}} \quad (2)$$

Mechanism 2

$$R_I = \frac{k_C C_E C_C}{1 + K_{E1} C_E + K_{P1} C_{P1}} \quad (3)$$

$$R_{II} = \frac{k_K C_E}{1 + K_{E2} C_E + K_{P2} C_{P2}} \quad (4)$$

Mechanism 3

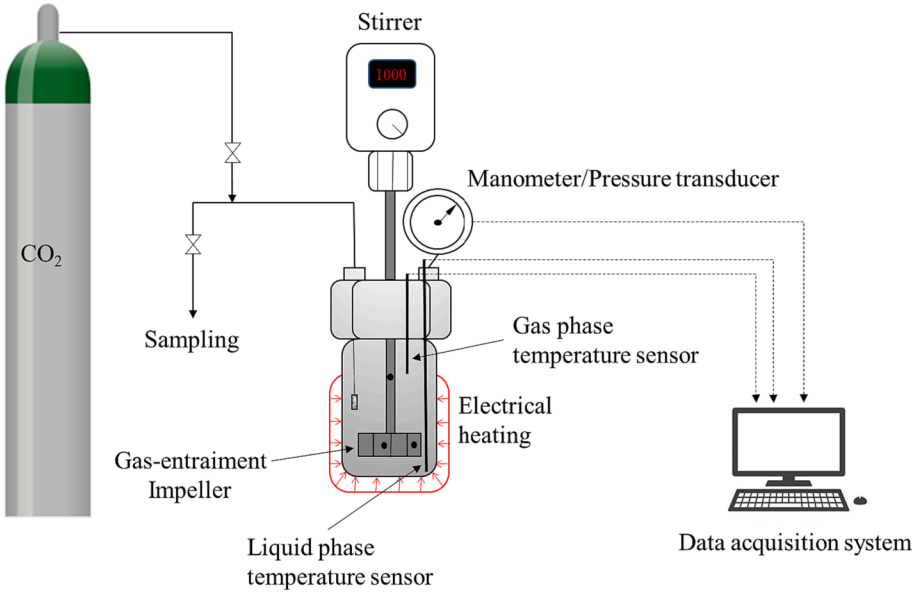

Fig. 3. Schematic view of the carbonation reactor system.

Table 2
Experimental matrix for the carbonation of EMO.

Reactor volume	0.327 L
Liquid Volume	0.055 L
Catalyst bulk density	27–110 g•L^{-1}
Stirring rate	800 rpm
Temperature	373–443 K
CO_2 pressure	20–60 bar

Table 3
Experimental matrix: gas–liquid mass transfer for EMO.

Exp No	P (bar)	T (K)	Stirring speed (RPM)
1	30	323.15	800
2	30	373.15	800
3	30	413.15	800
4	30	443.15	800
5	40	323.15	800
6	40	373.15	800
7	40	413.15	800
8	40	443.15	800
9	20	323.15	800
10	20	373.15	800
11	20	413.15	800
12	20	443.15	800

Notes: Substrate = EMO, No catalyst, $V_G = 0.055$ L, $V_L = 0.274$ L.

Table 4
Experimental matrix: gas–liquid mass transfer for CMO.

Exp No	P (bar)	T (K)	Stirring speed (RPM)
1	30	323.15	800
2	30	373.15	800
3	30	413.15	800
4	30	443.15	800
5	40	323.15	800
6	40	373.15	800
7	40	413.15	800
8	40	443.15	800

Notes: Substrate = CMO, No catalyst, $V_G = 0.051$ L, $V_L = 0.277$ L.

$$R_I = \frac{k_C C_E C_C}{(1 + K_{E1}C_E)(1 + K_{E2}C_E + K_{P1}C_{P1} + K_{P2}C_{P2})C_C + \alpha C_E} \quad (5)$$

$$R_{II} = \frac{k_K C_E C_C (1 + K_{E1}C_E)}{(1 + K_{E1}C_E)(1 + K_{E2}C_E + K_{P1}C_{P1} + K_{P2}C_{P2})C_C + \alpha C_E} \quad (6)$$

Mechanism 4

$$R_I = \frac{k_C C_E C_C}{1 + \alpha C_C + \gamma C_E + \beta C_E C_C + K_{P1}C_{P1} + P_{P2}C_{P2}} \quad (7)$$

$$R_{II} = \frac{k_K C_E}{1 + \alpha C_C + \gamma C_E + \beta C_E C_C + K_{P1}C_{P1} + K_{P2}C_{P2}} \quad (8)$$

Model 1 is mathematically a special case of Model 4, by setting α = 0 in Model 4, Model 1 is obtained.

Mechanism 5

$$R_I = \frac{k_C C_E C_C}{1 + K_{E1}C_E + K_{P1}C_{P1} + K_{P2}C_{P2}} \quad (9)$$

$$R_{II} = \frac{k_K C_E}{1 + K_{E1}C_E + K_{P1}C_{P1} + K_{P2}C_{P2}} \quad (10)$$

3.3. Generation rates of components

The consumption and production rates of the components are obtained from the reaction stoichiometry in a very straightforward way,

$$r_E = -R_I - R_{II} \quad (11)$$

$$r_C = -R_I \quad (12)$$

$$r_{P1} = R_I \quad (13)$$

$$r_{P2} = R_{II} \quad (14)$$

These generation rate expressions are implemented in the component mass balances for the reactor autoclave and they are useful in the product distribution analysis based on the models.

4. Reactor model

4.1. Basic principles

The basic principles of the reactor model can be understood by looking at the schematic view of the experimental device displayed in Fig. 3. New CO_2 was continuously fed into the vigorously stirred liquid phase, where the solid catalyst particles were immersed. In this way, the pressure of CO_2 in the gas phase was maintained constant throughout the experiment. From the modelling viewpoint, the system can be considered as a three-phase semibatch reactor: the solid catalyst and the liquid phases were in batch, while the gas phase was in semibatch mode. Because of vigorous stirring, the concentration and temperature gradients in the liquid phase vanished. Small catalyst particles were used and the reaction itself was slow, which implies that the external and internal mass transfer resistances around and inside the catalyst particles were suppressed. In this sense, the system worked under the conditions of intrinsic kinetics, but one question still remains: did the gas–liquid mass transfer resistance of CO_2 have an impact on the observed experimental results? To elucidate this very important issue, a series of experiments were conducted with different stirring rates. The experimental matrix is provided in Table 2. The experimental procedure and analytical methods are described in detail in our previous article (Perez Sena et al., 2022).

4.2. Component mass balances

The isothermal reactor model is written in such a way that the gas–liquid mass transfer effect is included in the balance equation of CO_2. The primary form of the gas-phase mass balance is (C═CO_2)

$$n'_{0GC} = N_C A + \frac{dn_{GC}}{dt} \quad (15)$$

where n = inlet molar flow of CO_2, N_C = diffusion flux of CO_2 into the liquid phase, A = gas–liquid surface area, n_{GC} = amount of CO_2 in the gas phase, t = time. Pure (99.995 %) CO_2 was used and the gas-phase volume and pressure were constant, because CO_2 was continuously added to the system and the total pressure was regulated.

For the liquid phase, the mass balance of CO_2 is written as

$$N_C A + r_C m_{cat} = \frac{dn_C}{dt} \quad (16)$$

where r_C = consumption rate of CO_2, m_{cat} = mass of catalyst, n_C = amount of CO_2 in the liquid phase. The description of the diffusion flux is an issue as such. A simple approach is to use the law of Fick along with the double-film (coupled gas and liquid films) theory for the modelling of the diffusion flux. This approximation is usually good enough to describe the diffusion of sparingly soluble gases in solvents (Salmi et al., 2019). Because the gas phase consisted always of pure CO_2, the diffusion resistance of CO_2 in the gas film did not exist. Based on this discourse, the flux expression for CO_2 in the liquid film is

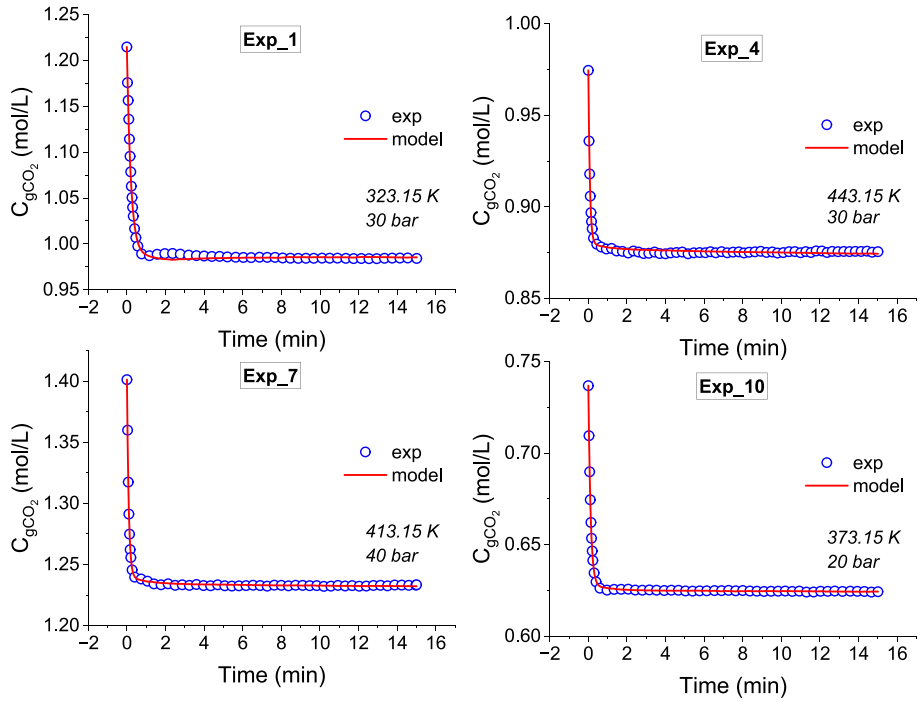

Fig. 4. Gas-liquid modelling results for epoxidized methyl oleate (EMO) at 800 rpm.

Table 5
Parameter estimation results: gas–liquid mass transfer for EMO.

Exp No	$k_L \bullet a_L$ (min^{-1})	K_H ($bar \bullet L \bullet mol^{-1}$)	R^2
1	3.78	17.47	0.98
2	7.74	31.83	0.99
3	9.90	42.43	0.99
4	12.12	53.85	0.97
5	3.89	18.11	0.99
6	7.38	33.75	0.98
7	10.19	44.95	0.99
8	11.84	51.99	0.99
9	4.25	16.78	0.99
10	7.37	30.24	0.99
11	9.22	42.56	0.99
12	9.80	55.55	0.98

$$N_C = k_{LC}(c^*_C - c_C) \tag{17}$$

where c^*_C denotes the saturation concentration of CO_2 at the gas–liquid interphase. For sparingly soluble gases, the law of Henry is applied for the gas solubility (Fogg and Gerrard, 1991; Salmi et al., 2019),

$$K_H = \frac{p^*_{GC}}{c^*_C} \tag{18}$$

from which the saturation concentration of CO_2 in the liquid phase (c^*_C) can be solved; $p^*_{CO2} = P$ in this case (pure gas),

$$c^*_C = \frac{P}{K_H} \tag{19}$$

The flux expression (40) becomes

$$N_C = k_{LC}\left(\frac{P}{K_H} - c_C\right) \tag{20}$$

The amount of substance is related to the concentration and the liquid volume,

$$n_C = c_C V_L \tag{21}$$

and the surface area-to-volume ratio (a_L) and the catalyst bulk density (ρ_B) are defined as follows,

$$a_L = \frac{A}{V_L} \tag{22}$$

$$\rho_B = \frac{m_{cat}}{V_L} \tag{23}$$

After inserting these quantities in Eq. (16), the mass balance of CO_2 gets the form

$$\frac{dc_C}{dt} = k_{LC}a_L\left(\frac{P}{K_H} - c_C\right) + r_C\rho_B \tag{24}$$

For the non-volatile liquid-phase components, the epoxide (E) and the carbonated product (P1) and the ketone (P2), the gas–liquid flux is zero and the balance equations become

$$r_i m_{cat} = \frac{dn_i}{dt} \tag{25}$$

where i = E or i = P1, P2. For a constant liquid-phase volume, the balance equation can be simplified to

$$\frac{dc_i}{dt} = r_i\rho_B \tag{26}$$

The model Eqs. (24) and (26) form a system of ordinary differential equations (ODEs), an initial value problem (IVP) which has the following initial conditions at $t = 0$,

$$c_i = c_{0i} \tag{27}$$

where i = C, E, P.

4.3. Gas-liquid mass transfer mass balance

The mass transfer parameter $k_L a_L$ and Henry's constant K_H can be obtained by performing individual experiments in the absence of the catalyst, i.e. in the absence of chemical reactions. In this case, the mass

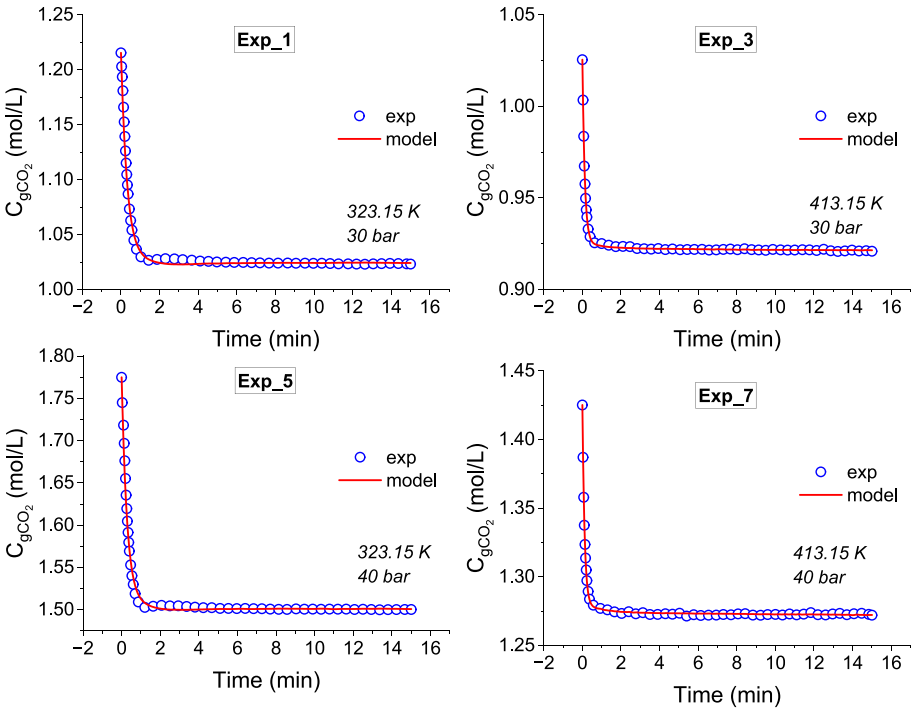

Fig. 5. Gas-liquid mass transfer modelling results for carbonated methyl oleate (CMO) at 800 rpm.

Table 6
Parameter estimation results for gas–liquid mass transfer of CMO.

Exp No	$k_L a_L$ (min^{-1})	K_H (bar•L•mol^{-1})	R^2
1	2.52	20.74	0.98
2	6.21	36.13	0.99
3	7.53	48.93	0.99
4	9.73	52.09	0.99
5	2.92	22.08	0.98
6	6.11	37.34	0.98
7	8.18	45.23	0.99
8	11.41	49.25	0.91

balances of the components in the system become

$$\frac{dc_C}{dt} = k_{LC}a_L\left(\frac{P}{K_H} - c_C\right) \tag{28}$$

$$\frac{dc_i}{dt} = 0 \tag{29}$$

where i refers to the liquid-phase components. The parameters $k_L a_L$ and K_H can be obtained from Eq. (28) if the concentration of CO_2 in the liquid phase is followed. Otherwise, during the experiments, the CO_2 pressure and temperature are accurately monitored in the gas phase, therefore, the gas phase mass balance is preferred for the task,

$$\frac{dc_{GC}}{dt} = -k_{LC}a_G\left(\frac{P}{K_H} - c_C\right) \tag{30}$$

The main differences between Eqs. (28) and (30) is that $a_G = A/V_G$. Multiplication by V_G/V_L can easily transform the $k_L a_G$ parameter to $k_L a_L$, which is more practical in the estimation of the kinetic parameters, where the liquid-phase mass balances (24) and (26) are used.

The gas-phase concentration of CO_2(c_{GC}) is obtained from an equation of state (EoS), a non-ideal gas law,

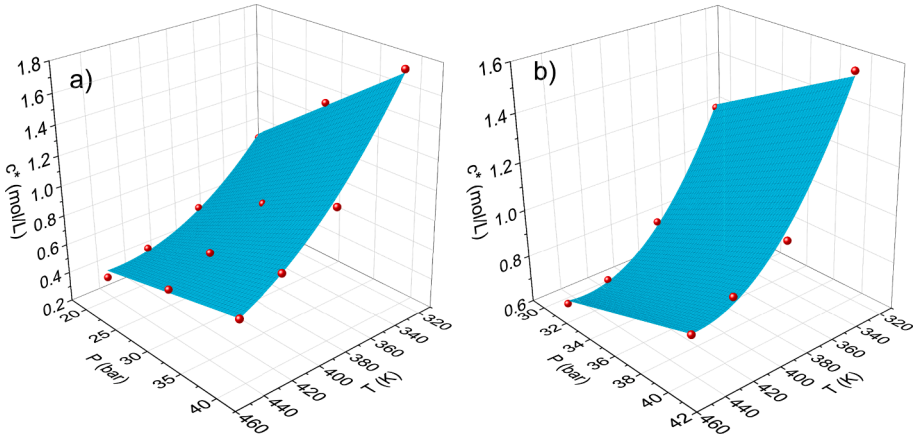

Fig. 6. Saturation concentration (solubility) of CO_2 in the liquid phase as a function of pressure and temperature: a) EMO and b) CMO.

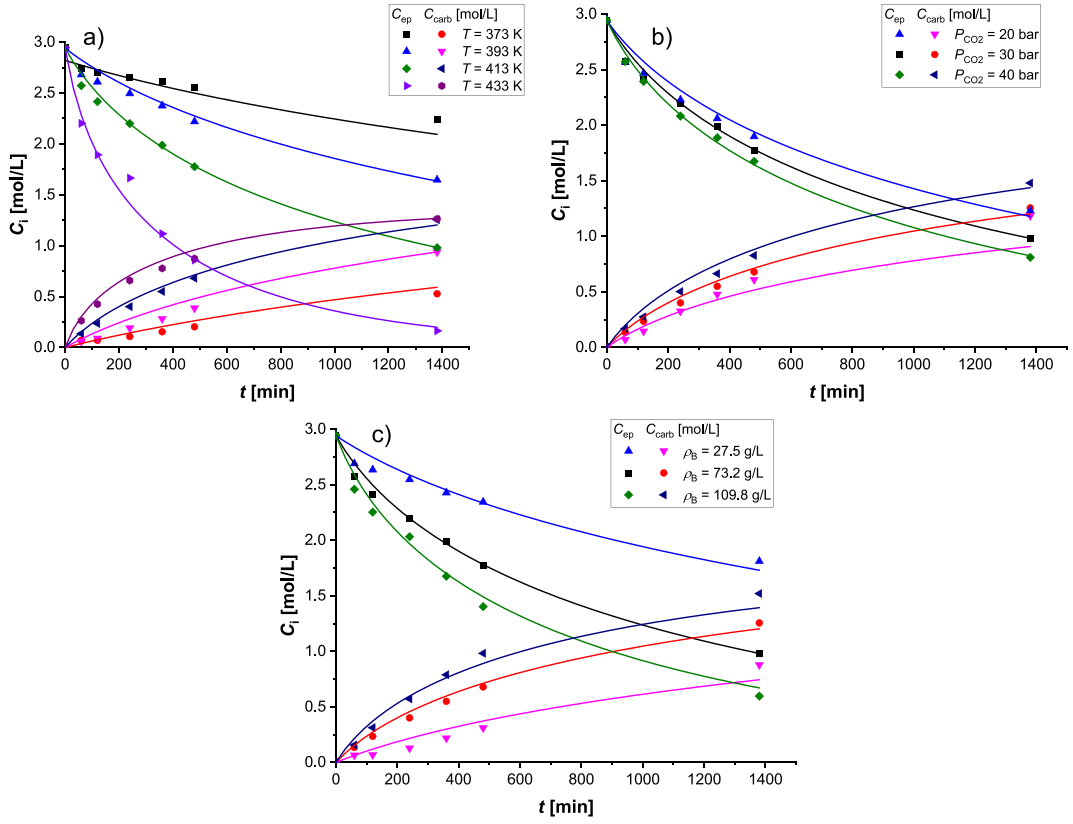

Fig. 7. Fit of the model to the experimental data for the mechanism 1: a) temperature, b) pressure and c) catalyst bulk density.

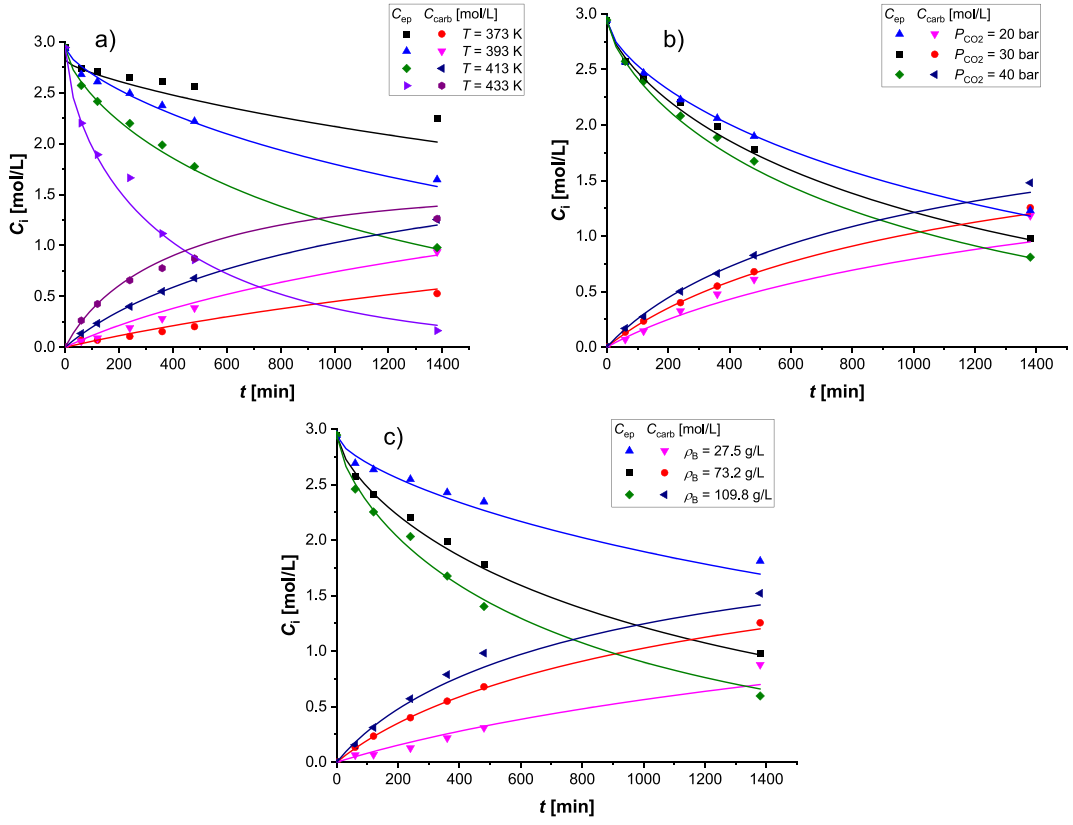

Fig. 8. Fit of the model to the experimental data for the mechanism 2: a) temperature, b) pressure and c) catalyst bulk density.

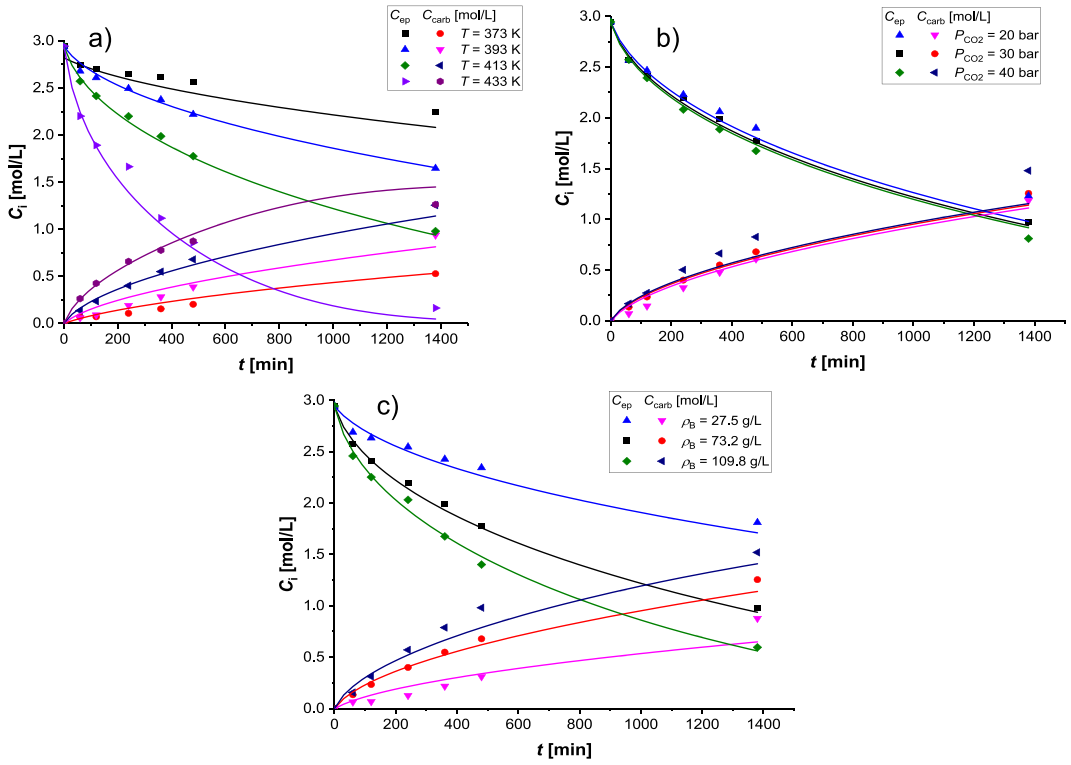

Fig. 9. Fit of the model to the experimental data for the mechanism 3: a) temperature, b) pressure and c) catalyst bulk density.

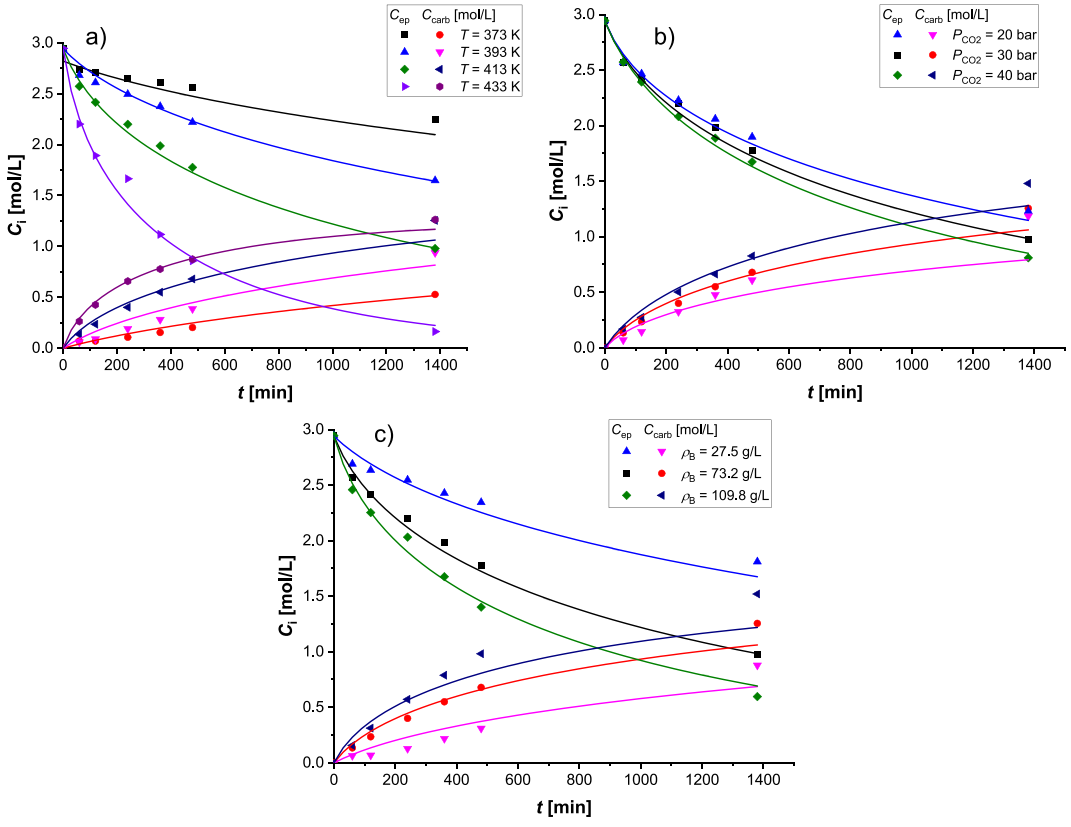

Fig. 10. Fit of the model to the experimental data for the mechanism 4: a) temperature, b) pressure and c) catalyst bulk density.

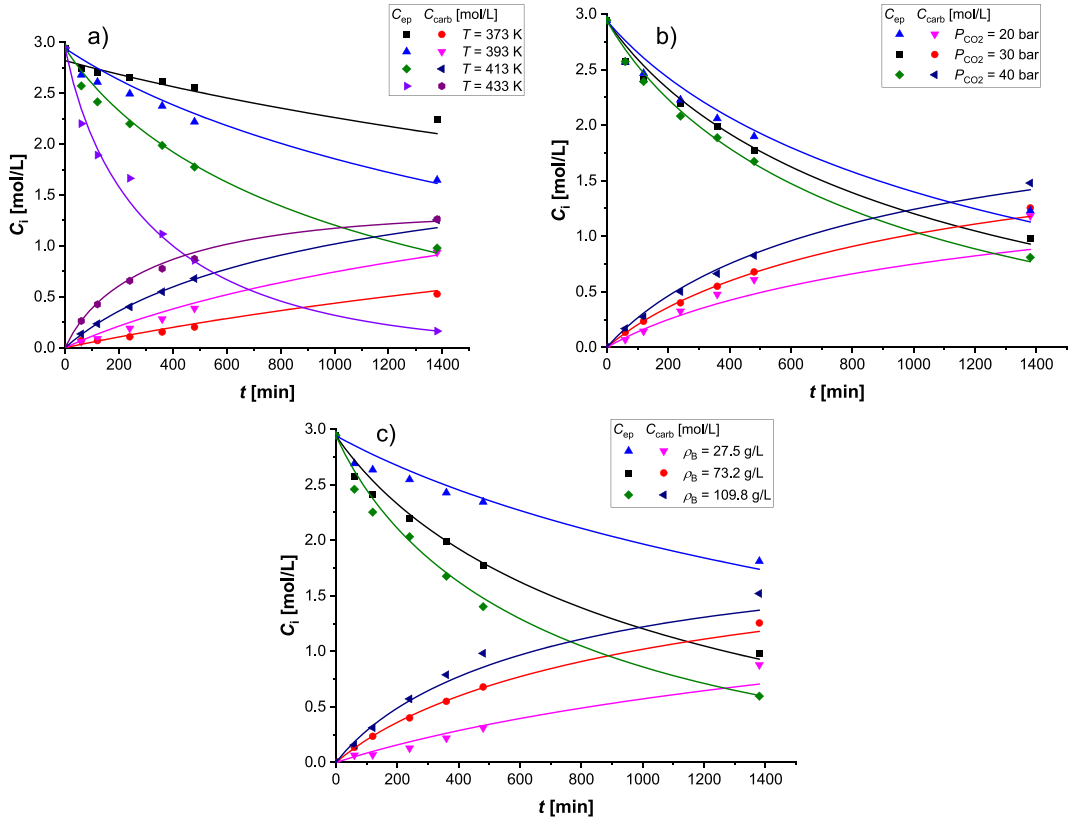

Fig. 11. Fit of the model to the experimental data for the mechanism 5: a) temperature, b) pressure and c) catalyst bulk density.

Table 7
Parameter estimation results for mechanism 1.

Parameter	Unit	Value	Est. relative Std Error (%)
k_C	$L^2 \cdot mol^{-1} \cdot g^{-1} \cdot min^{-1}$	2.06E−05	23.9
k_K	$L \cdot g^{-1} \cdot min^{-1}$	8.75E−06	23.5
α	$L \cdot mol^{-1}$	1.38E−07	>100
β	$L^2 \cdot mol^{-2}$	1.00E−03	>100
K_{P1}	$L \cdot mol^{-1}$	7.78E−01	43.9
K_{P2}	$L \cdot mol^{-1}$	1.18E+00	69.3
Ea_{kc}	$J \cdot mol^{-1}$	5.72E+04	5.2
Ea_{kk}	$J \cdot mol^{-1}$	7.94E+04	5.9

$$c_{GC} = \frac{P}{ZRT} \tag{31}$$

and the compressibility factor Z is estimated by using Peng-Robinson (PR) equation of state in its very compact cubic form (Reid et al., 1988),

$$Z^3 - (1-B)Z^2 + (A - 2B - 3B^2)Z - (AB - B^2 - B^3) = 0 \tag{32}$$

where A and B are

$$A = \frac{aP}{(R_G T)^2} \tag{33}$$

$$B = \frac{bP}{R_G T} \tag{34}$$

Parameters α, a and are dependent on the physical properties of the gas (Reid et al., 1988), Eq. (32) can be solved relatively rapidly and it provides a very satisfactory prediction for CO_2 at the investigated

Table 9
Parameter estimation results for mechanism 2.

Parameter	Unit	Value	Est. relative Std Error (%)
k_c	$L^2 \cdot mol^{-1} \cdot g^{-1} \cdot min^{-1}$	1.62E−05	>100
k_k	$L \cdot g^{-1} \cdot min^{-1}$	8.57E−04	29
K_{E1}	$L \cdot mol^{-1}$	1.15E−05	>100
K_{E2}	$L \cdot mol^{-1}$	1.39E−05	>100
K_{P1}	$L \cdot mol^{-1}$	7.92E−01	>100
K_{P2}	$L \cdot mol^{-1}$	4.60E+02	29.5
Ea_{kc}	$J \cdot mol^{-1}$	5.18E+04	5.5
Ea_{kk}	$J \cdot mol^{-1}$	8.87E+04	6.3

Table 8
Correlation matrix of the kinetic parameters for mechanism 1.

	k_c	k_k	A	β	K_{P1}	K_{P2}	Ea_{kc}	Ea_{kk}
k_c	1.000							
k_k	0.970	1.000						
α	−0.018	−0.030	1.000					
β	0.955	0.943	−0.151	1.000				
K_{P1}	0.275	0.240	−0.135	0.215	1.000			
K_{P2}	0.805	0.799	0.033	0.755	−0.305	1.000		
Ea_{kc}	0.135	0.155	0.150	0.038	−0.571	0.563	1.000	
Ea_{kk}	0.176	0.059	0.143	0.087	−0.304	0.401	0.430	1.000

Table 10
Correlation matrix of the kinetic parameters for mechanism 2.

	k_c	k_k	K_{E1}	K_{E2}	K_{P1}	K_{P2}	Ea_{kc}	Ea_{kk}
k_c	1							
k_k	−0.54	1						
K_{E1}	0.998	−0.53	1					
K_{E2}	−0.056	0.222	−0.056	1				
K_{P1}	0.997	−0.542	0.992	−0.046	1			
K_{P2}	−0.549	0.972	−0.55	0.106	−0.544	1		
Ea_{kc}	−0.676	0.478	−0.679	0.106	−0.66	0.482	1	
Ea_{kk}	0.4	−0.881	0.387	−0.324	0.401	−0.815	−0.649	1

Table 11
Parameter estimation results for mechanism 3.

Parameter	Unit	Value	Est. relative Std Error (%)
k_c	$L{\cdot}g^{-1}{\cdot}min^{-1}$	3.10E−04	49.1
k_k	$L{\cdot}g^{-1}{\cdot}min^{-1}$	4.84E−05	24.8
α	$L{\cdot}mol^{-1}$	1.70E+00	52.7
K_{E1}	$L{\cdot}mol^{-1}$	2.04E+00	57.3
K_{E2}	$L{\cdot}mol^{-1}$	3.37E−08	>100
K_{P1}	$L{\cdot}mol^{-1}$	2.38E−03	>100
K_{P2}	$L{\cdot}mol^{-1}$	1.65E+01	60.7
Ea_{kc}	$J{\cdot}mol^{-1}$	6.69E+04	13.8
Ea_{kk}	$J{\cdot}mol^{-1}$	9.52E+04	9.8
Ea_{α}	$J{\cdot}mol^{-1}$	4.96E+04	26.2

operation conditions.

A critical remark is however necessary: the change of the physical properties during the reaction, especially the liquid viscosity might influence the diffusion coefficient – and consequently, the mass transfer coefficient of CO_2 in the liquid phase during the reaction. The mass transfer parameter $k_L a_L$ most probably decreases during the experiment and also the solubility constant K_H might be influenced by the gradual chemical changes in the reaction milieu. For this reason, two sets of mass transfer experiments were carried out using epoxidized methyl oleate and previously synthesized carbonated methyl oleate. The experimental matrices are displayed in Tables 3 and 4, respectively.

4.4. Product distribution analysis

Before taking the big leap to parameter estimation by nonlinear regression, a product distribution analysis is useful to gain additional understanding on the reaction system. In this sense, the rate equations belong to two categories, models with common denominators for the product formation (models 1, 4 and 5) and models with different denominators in the rate equations (models 2 and 3). The basic assumption in the product distribution analysis is that the system operates under kinetic control and under constant carbon dioxide pressure, which means that the mass balance of carbon dioxide can be discarded.

The general liquid-phase mass balance Eq. (26) is valid for the reaction products (P1 and P2); taking into account the generation rate Eqs. (13) and (14), we get

$$\frac{dc_{P1}}{dt} = R_I \rho_B \tag{35}$$

$$\frac{dc_{P2}}{dt} = R_{II} \rho_B \tag{36}$$

Elimination of the reaction time gives

$$\frac{dc_{P1}}{dc_{P2}} = \frac{R_I}{R_{II}} \tag{37}$$

For models 1, 4 and 5, equation (37) becomes

$$\frac{dc_{P1}}{dc_{P2}} = \alpha' c_{CO2} \tag{38}$$

where α' is a merge of fundamental model parameters, i.e. rate and equilibrium constants. The detailed content of α' depends on the particular model. In general, α' is temperature dependent, but for one temperature and carbon dioxide pressure, a lump can be used,

$$\omega' = \alpha' c_{CO2} \tag{39}$$

Separation of variables and integrating Eq. (38) with the limits [0, c_{P1}] and [0,c_{P2}] gives a linear relationship

$$c_{P2} = c_{P1}/\omega' \tag{40}$$

Table 13
Parameter estimation results for mechanism 4.

Parameter	Unit	Value	Est. relative Std Error (%)
k_C	$L^2{\cdot}mol^{-1}{\cdot}g^{-1}{\cdot}min^{-1}$	6.24E−05	47
k_K	$L{\cdot}g^{-1}{\cdot}min^{-1}$	3.55E−05	46.9
α	$L{\cdot}mol^{-1}$	1.87E−02	>100
γ	$L{\cdot}mol^{-1}$	3.99E−05	>100
β	$L^2{\cdot}mol^{-2}$	6.77E−01	86.3
K_{P1}	$L{\cdot}mol^{-1}$	2.60E+00	75.4
K_{P2}	$L{\cdot}mol^{-1}$	6.96E+00	95.6
Ea_{kc}	$J{\cdot}mol^{-1}$	6.74E+04	22.4
Ea_{kk}	$J{\cdot}mol^{-1}$	8.13E+04	18.7
Ea_{α}	$J{\cdot}mol^{-1}$	2.26E+05	>100
Ea_{γ}	$J{\cdot}mol^{-1}$	1.39E+05	>100
Ea_{β}	$J{\cdot}mol^{-1}$	1.71E+04	>100

Table 12
Correlation matrix of the kinetic parameters for mechanism 3.

	k_c	k_k	α	K_{E1}	K_{E2}	K_{P1}	K_{P2}	Ea_{kc}	Ea_{kk}	Ea_{α}
k_c	1									
k_k	0.29	1								
α	0.951	0.505	1							
K_{E1}	0.871	−0.214	0.713	1						
K_{E2}	0.093	0.163	0.064	0.012	1					
K_{P1}	0.136	−0.686	0.008	0.487	−0.046	1				
K_{P2}	0.09	0.89	0.252	−0.366	0.126	−0.933	1			
Ea_{kc}	0.014	0.837	0.181	−0.417	−0.001	−0.909	0.954	1		
Ea_{kk}	0.081	0.806	0.231	−0.342	0.027	−0.845	0.915	0.964	1	
Ea_{α}	0.043	0.539	0.13	−0.24	−0.312	−0.612	0.639	0.816	0.832	1

Table 14
Correlation matrix of the kinetic parameters for mechanism 4.

	k_c	k_k	α	γ	B	K_{P1}	K_{P2}	Ea_{kc}	Ea_{kk}	Ea_{α}	Ea_{γ}	Ea_{β}
k_c	1											
k_k	0.997	1										
α	−0.083	−0.086	1									
γ	0.098	0.1	−0.227	1								
β	0.944	0.943	−0.383	0.063	1							
K_{P1}	−0.49	−0.5	−0.253	0.39	−0.438	1						
K_{P2}	0.965	0.966	−0.037	−0.034	0.912	−0.685	1					
Ea_{kc}	0.388	0.388	0.329	−0.166	0.287	−0.579	0.462	1				
Ea_{kk}	0.394	0.385	0.33	−0.165	0.288	−0.559	0.46	0.984	1			
Ea_{α}	0.1	0.103	−0.986	0.218	0.4	0.21	0.058	−0.19	−0.194	1		
Ea_{γ}	0.004	0.005	−0.19	−0.209	0.061	0.111	0.013	−0.728	−0.71	0.032	1	
Ea_{β}	0.252	0.252	−0.038	−0.186	0.288	−0.443	0.321	0.897	0.883	0.186	−0.729	1

Table 15
Parameter estimation results for mechanism 5.

Parameter	Unit	Value	Est. relative Std Error (%)
k_C	$L^2 \cdot mol^{-1} \cdot g^{-1} \cdot min^{-1}$	0.163E−04	2.3
k_K	$L \cdot g^{-1} \cdot min^{-1}$	0.775E−05	5.9
K_{E1}	$L \cdot mol^{-1}$	0.377E−09	>100
K_{P1}	$L \cdot mol^{-1}$	0.426E+00	42.2
K_{P2}	$L \cdot mol^{-1}$	0.682E+00	35.5
Ea_{kc}	$J \cdot mol^{-1}$	0.551E+05	2.6
Ea_{kk}	$J \cdot mol^{-1}$	0.746E+05	4.8

Table 16
Correlation matrix of the kinetic parameters for mechanism 5.

	k_c	k_k	K_{E1}	K_{P1}	K_{P2}	Ea_{kc}	Ea_{kk}
k_c	1						
k_k	0.631	1					
K_{E1}	0.359	0.241	1				
K_{P1}	0.297	0.068	0.029	1			
K_{P2}	0.269	0.239	0.19	−0.81	1		
Ea_{kc}	0.364	0.278	0.377	−0.488	0.749	1	
Ea_{kk}	0.011	−0.416	0.178	−0.011	0.036	0.422	1

By plotting c_{P2} vs c_{P1} it can be checked, whether the proposed rate equation can be valid. Moreover, the reaction order with respect to CO_2 can be investigated by plotting the ω'-values as a function of the CO_2 concentration (or partial pressure) separately at different temperatures. In this way, a preliminary estimation of the merged parameter α' can be obtained.

Model 3 is a very interesting case. Division of the balance equations of P1 and P2 gives

$$\frac{dc_{P2}}{dc_{P1}} = \omega(1 + K_E c_E) \tag{41}$$

The total balance of the species is

$$c_{0E} = c_E + c_{P1} + c_{P2} \tag{42}$$

assuming that the amount of adsorbed species is small compared to the amount of substance in the liquid phase. The concentration of c_E is solved from equation (42) and inserted in Eq. (41). The differential equation

$$\frac{dc_{P2}}{dc_{P1}} = (k_K/k_C)(1 + K_E(c_{0E} - c_{P1} - c_{P2})) \tag{43}$$

gives the relation between the product concentrations. A substitution z = c_{P1} + c_{P2} is introduced, which implies that

$$\frac{dz}{dc_{P1}} = 1 + \frac{dc_{P2}}{dc_{P1}} \tag{44}$$

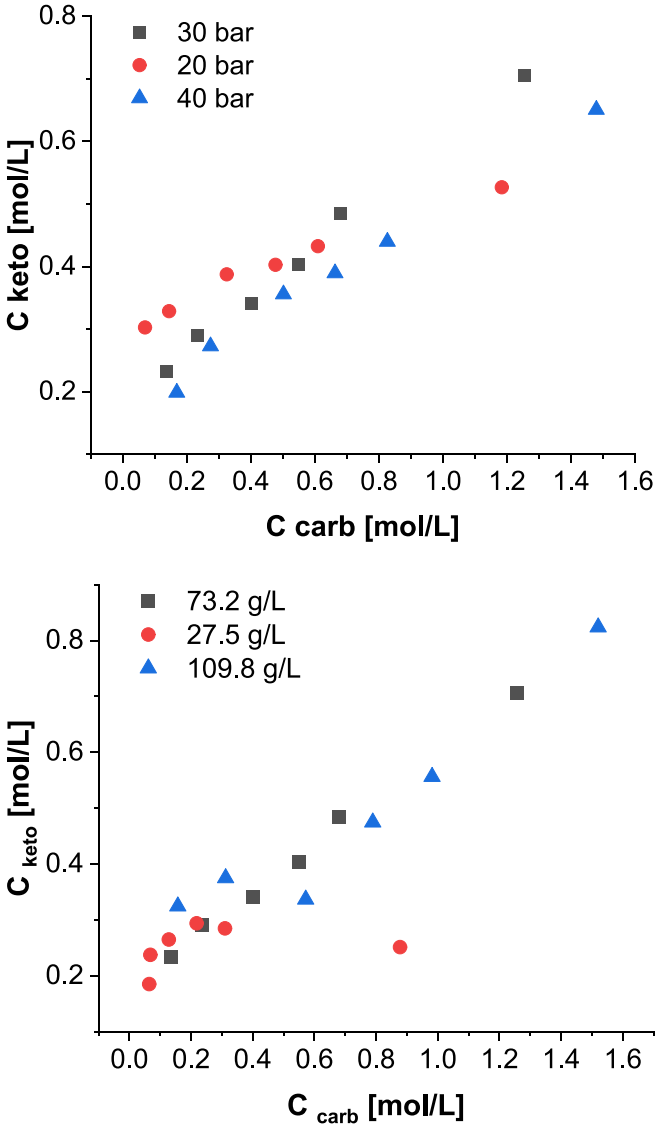

Fig. 12. Product distribution analysis: the effect of carbon dioxide pressure (upper) and the effect of the catalyst bulk density (lower).

This relation is inserted in Eq. (43) giving

$$\frac{dz}{dc_{P1}} - 1 = \alpha' - \beta' z \tag{45}$$

Separation of variables and integration with the limits [0,z] and [0,c_{P1}]

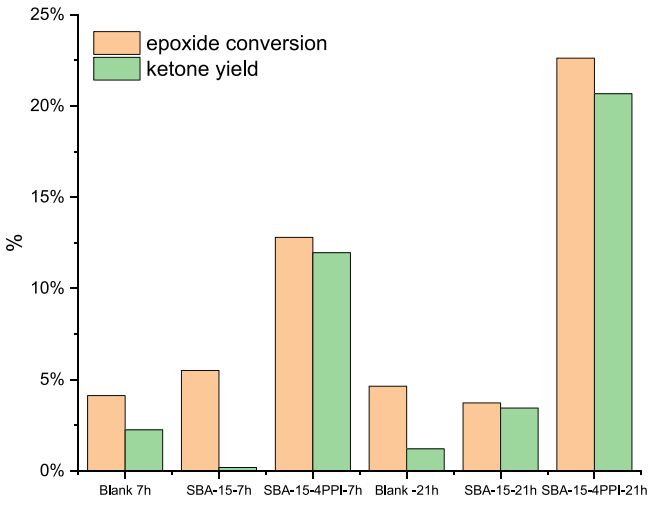

Fig. 13. Ketonisation efficiency of different catalysts.

gives the analytical solution

$$-\ln\frac{1+\alpha'-\beta'(c_{P1}+c_{P2})}{1+\alpha'}=\beta' c_{P1} \tag{46}$$

i.e.

$$c_{P2}=\frac{(1+\alpha')(1-\exp(-\beta' c_{P1}))}{\beta'}-c_{P1} \tag{47}$$

For the limit case, β'=0, and by applying the rule of L'Hôpital it can be shown that Eq. (47) shrinks to the simple linear expression (40).

4.5. Analytical solution of the epoxide mass balances

A very interesting special case appears when the carbonation reaction is carried out under vigorous stirring and the CO_2 concentration in the liquid phase is kept constant by continuous and regulated addition. This implies that the mass balance equation of the epoxide species can be written in the general form for all the kinetic models 1–5,

$$\frac{dc_E}{dt}=-\left(\frac{\alpha_1}{1+\beta_1 c_E}+\frac{\alpha_2}{1+\beta_2 c_E}\right)c_E \tag{48}$$

where the merged parameters depend on the specific case. Eq. (48) can be used for all the mechanisms presented, but $\alpha_2 = 0$ for mechanisms 1, 3, 4 and 5. The differential Eq. (48) is solved analytically with respect to the epoxide concentration (c_E) and the reaction time (t).

Separation of the variables gives the integration problem

$$\int_{cE}^{c0E}\frac{(1+\beta_1 c_E)(1+\beta_2 c_E)dc_E}{c_E(\alpha_1(1+\beta_2 c_E)+\alpha_2(1+\beta_1 c_E))}=\int_0^t dt \tag{49}$$

The left-hand side of Eq. (49) is developed to partial fractions and integrated within the limits [0, t] and [c_E, c_{0E}]. The solution becomes (Supplementary information)

$$\frac{\alpha}{\omega}(c_{0E}-c_E)+\left(\frac{\beta-\omega-\alpha/\omega}{\omega}\right)\ln\left(\frac{1+\omega c_{0E}}{1+\omega c_E}\right)+\ln\left(\frac{c_{0E}}{c_E}\right)=(\alpha_1+\alpha_2)t \tag{50}$$

Introduction of the dimensionless concentration $y = c_E/c_{0E}$ gives

$$\frac{\alpha c_{0E}}{\omega}(1-y)+\left(\frac{\beta-\omega-\alpha/\omega}{\omega}\right)\ln\left(\frac{1+\omega c_{0E}}{1+\omega c_{0E}y}\right)-\ln y=(\alpha_1+\alpha_2)t \tag{51}$$

Eq. (51) can be written in a very compact parametric form

$$\kappa(1-y)+\lambda\ln\left(\frac{1+\delta}{1+\delta y}\right)-\ln y=\gamma t \tag{52}$$

where

$$\alpha=\beta_1\beta_2 \tag{53}$$

$$\beta=\beta_1+\beta_2 \tag{54}$$

$$\omega=\frac{\alpha_1\beta_2+\alpha_2\beta_1}{\alpha_1+\alpha_2} \tag{55}$$

$$\kappa=\frac{\alpha c_{0E}}{\omega} \tag{56}$$

$$\lambda=\frac{\beta-\omega-\alpha/\omega}{\omega} \tag{57}$$

$$\delta=\omega c_{0E} \tag{58}$$

$$\gamma=\alpha_1+\alpha_2 \tag{59}$$

The model parameters δ, κ, and λ are dimensionless, while γ has the dimension of reciprocal time (min^{-1}).

Some limit cases of the general solution (51) are of interest. For only one type of active sites, the model is simplified. For instance, if $\alpha_2 = 0$, then $\omega = \beta_2$, $\kappa = \beta_1 c_{0E}$, $\lambda = 0$, $\gamma = \alpha_1$ and equation (52) shrinks to

$$\kappa(1-y)-\ln y=\gamma t \tag{60}$$

In case of weak adsorption of the components, κ and λ in Eq. (52) are zero and a simple exponential function is obtained.

Eqs. (52) and (60) can be used to investigate the parameter estimation results: a plot of the left-hand side of these equations versus the reaction time (t) should give a straight line if the model is valid.

4.6. Summary of model equations and numerical strategies

The mathematical model consists of the rate Eqs. (1)–(10), the component generation rate expressions (11)–(14) and the mass balances (24) and (26) along with the initial conditions (27). This system of coupled ordinary differential equations (ODEs) was solved numerically as an initial value problem (IVP) with a stiff ODE solver implemented in the software package ModEst (Haario, 2014). The values of the rate and adsorption parameters were varied systematically to obtain the best possible fit of the model to the experimental data. The search for the optimal parameter values was done with the aid of a hybrid simplex-Levenberg-Marquardt algorithm implemented in the software ModEst. The ODE solver worked under the optimization routine to provide the model predictions, i.e. the concentration curves at different parameter values. As the best fit of the model to the experimental data, the minimum of the residual sum of squares (Q) was accepted,

$$Q=\sum(c_{i,t}-c_{i\exp,t})^2 \tag{61}$$

where the subscript exp,t refers to the experimentally recorded concentrations of E and P at different reaction times. The concentrations $c_{i,t}$ were provided from the model predictions, from Eq. (26). Besides the standard statistical analysis, i.e. the errors of the parameters and the correlation matrices, a Markov Chain Monte Carlo (MCMC) method was used to investigate the probability distributions of the estimated parameters (Haario et al., 2001).

5. Modelling results and discussion

5.1. 1 Gas-liquid mass transfer

The results from the gas–liquid mass transfer experiments of CO_2 into epoxidized methyl oleate (Table 3) are shown in Fig. 4. An excellent fit of equation (30) was achieved for all the experiments performed. The results displayed in Fig. 4 suggest that the gas–liquid mass transfer

proceeds very rapidly; after two minutes, the liquid phase was saturated with CO_2. The estimated volumetric mass transfer coefficient and Henry's constant are given in Table 5.

Additional gas–liquid mass transfer experiments (Table 4) were conducted using a previously synthesized carbonated methyl oleate (CMO) as the liquid phase to obtain a better estimation of the volumetric mass transfer coefficient and Henry's constant during the course of the reaction. Fig. 5 shows the fit of the model to the CO_2 concentration in the gas phase. The CMO mass transfer results displayed in Fig. 5 exhibit very a similar behavior to the EMO mass transfer results, reaching the near-saturation concentration of CO_2 after two minutes. The estimated mass transfer parameters for CMO are listed in Table 6.

It is worth mentioning that the volumetric mass transfer coefficient and the Henry's constant are known to depend strongly on the physical properties of the liquid, in which the gas diffuses and dissolves (i.e. viscosity, density), and these properties are influenced by the temperature and pressure as clearly indicated by the varying results of both parameters under different experimental conditions and compositions of the liquid phases (Tables 5 and 6). Therefore, it is necessary to introduce weighted averages for the mass transfer coefficient and the Henry's constant to account for their changes during the experiment (i.e. EMO → CMO),

$$(k_La_L)_{mix} = (k_La_L)_{EMO}\cdot x_{EMO} + (1 - x_{EMO})\cdot(k_La_L)_{CMO} \tag{62}$$

$$(K_H)_{mix} = (K_H)_{EMO}\cdot x_{EMO} + (1 - x_{EMO})\cdot(K_H)_{CMO} \tag{63}$$

The solubility of CO_2 in epoxidized methyl oleate and carbonated methyl oleate was calculated from the change of the CO_2 concentration in the gas phase during the mass transfer experiment. The effect of temperature and pressure on the solubility is displayed in Fig. 6. As expected, a very pronounced temperature effect on the solubility is observed in both cases, EMO and CMO, while a less pronounced impact is observed with the change of the pressure. Based on the results shown in Fig. 6, the solubility of CO_2 in EMO and CMO can be expressed as a function of temperature and pressure,

$$C^*_{CO_2}(EMO) = 6.34253 + 0.11011P - 0.03269T + 4.23904e^{-5}T^2 - 2.22456e^{-4}PT(mol/L) \tag{64}$$

$$C^*_{CO_2}(CMO) = 8.66014 + 0.06587P - 0.04358T + 5.41e^{-5}T^2 - 1.02809e^{-4}PT(mol/L) \tag{65}$$

5.2. Kinetic modelling results and discussion

The experimental results and the model predictions for mechanisms 1–5 are collected in Figs. 7–11. Some typical features can be seen in these figures. A profound effect of the reaction temperature and the catalyst amount is visible in the results, while the effect of carbon dioxide concentration is rather minor, but observable. However, thanks to the many experiments and repetition of them, it is undeniable that a pressure effect exists: an increase of the carbon dioxide pressure gives a slight enhancement of the carbonation rate.

In the comparison of the rival models, the following characteristics can be considered: residual sum of squares (Q), degree of explanation (R^2), parameter errors, and correlation between the parameters. In the final stage, the MCMC analysis gives indication on the probability distributions of the estimated parameters. In general, the kinetic models for all the mechanisms gave a rather good description of the experimental data with a degree of determination (R^2) around 99 %, as can be confirmed by looking at the fit of the predicted concentrations to the experimental data. An essential feature is the adsorption of the reaction products (P1 and P2) on the catalyst. If these adsorption parameters are discarded, the model fit is clearly impaired in most cases. The carbon dioxide pressure effect was explained well by proposed the models except model 3. The rapid decrease of the epoxide concentration was described well by all the models. The parameter values along with the estimation statistics are given in Tables 7–16. The number of adjustable parameters differs from model to model: models 1 and 2 have 8 parameters, model 3 has 10 parameters, model 4 has 12 parameters, while model has 7 parameters. The increase of the number of adjustable parameters did not bring any essential improve of the fit, but it impaired the estimation statistics, i.e. the standard errors of the parameters as well the mutual correlations.

The MCMC plots (Supplementary Information) reveal the probability distributions of the individual parameters. Model 5 has the smallest number of parameters and this fact is demonstrated in the MCMC analysis: all the parameters of model 5 have a probability with a well-defined maximum.

The product distribution analysis was applied on the primary concentration data as described in Section 4.3. The plots of the carbonated (P1) versus the ketone (P2) product are shown in Fig. 12. The plots are rather linear and dependent on the carbon dioxide pressure, as predicted by equations (39)-(40), which gives support to the proposed mechanisms 1, 4 and 5. Fig. 12 shows that the plots are independent of the mass of catalyst, which confirms the operation within the regime of intrinsic kinetics. The product distribution was practically constant during the experiments with different catalyst amounts as depicted in Fig. 12, thus confirming that Eq. (40) can be used to describe the product distribution at a constant carbon dioxide pressure. The selectivity of the carbonate product was around 63 % (Fig. 12, lower image).

The general conclusion is that all the models presented can well be used for engineering purposes. To advance in the chemical understanding of the system, additional experiments were conducted in the absence of carbon dioxide. In this way, the carbonation path is eliminated, but the formation of ketone is expected. A comparison of the ketone formation on different catalysts is provided in Fig. 13. The results are unequivocal: the catalyst with nucleophilic sites is superior (catalyst SBA-15-4PPI-21 h), which gives a very strong indication that the ketone is predominantly formed on the nucleophilic site. Thus, from the chemical viewpoint, models 3–5 should be preferred to models 1 and 2. From the viewpoint of pure statistics, model 5 could be favored, because it has the lowest number of adjustable parameters. On the other hand, considering the interaction between the Lewis and nucleophilic sites, model 4 can be regarded more probable from the chemical viewpoint.

6. Conclusions

An extensive experimental and modelling effort of epoxide carbonization was carried out in a laboratory-scale semibatch reactor. The catalyst contained both Lewis and nucleophilic sites, which gave inspiration for a detailed study of these sites and their mutual interaction. Experimental data were produced, describing the carbon dioxide solubility and mass transfer, the carbonation kinetics and the product distribution. Five rival reaction mechanisms were compared by nonlinear regression analysis and the formation of the side product, the ketone was studied in separate experiments in the absence of carbon dioxide. The results indicated that the dominant path to the ketone proceeds via the nucleophilic sites. As a final conclusion, it can be stated that the carbonation requires an interaction of the Lewis sites and the nucleophilic sites, while the ketone formation can proceed in the absence of the Lewis sites. For practical engineering purposes, the model which assumes a parallel formation of the epoxide and the ketone on the nucleophilic sites (model 5) is very useful, even though it can be regarded as an approximation from the strictly chemical viewpoint. The work could in future be expanded to other model molecules and mixtures of epoxides.

CRediT authorship contribution statement

Tapio Salmi: Conceptualization, Formal analysis, Funding acquisition, Methodology, Project administration, Supervision, Writing –

original draft, Writing – review & editing. **Wander Y. Perez-Sena:** Conceptualization, Data curation, Formal analysis, Investigation, Methodology, Supervision, Writing – original draft. **Fabrizio Ciccarelli:** Data curation, Formal analysis, Investigation. **Kari Eränen:** Conceptualization, Data curation, Investigation, Methodology, Project administration, Supervision. **Ananias Medina:** . **Tommaso Cogliano:** . **Martino Di Serio:** Conceptualization, Methodology, Project administration, Supervision. **Johan Wärnå:** Formal analysis, Methodology, Supervision. **Sébastien Leveneur:** . **Vincenzo Russo:** .

Declaration of competing interest

The authors declare that they have no known competing financial interests or personal relationships that could have appeared to influence the work reported in this paper.

Data availability

Data will be made available on request.

Acknowledgement

This work is part of the activities of Johan Gadolin Process Chemistry Centre (PCC). The research is financed by Academy of Finland, the Academy Professor grants 319002, 320115, 345053 (T. Salmi and W. Perez-Sena). The economic support is gratefully acknowledged.

Appendix A. Supplementary data

Supplementary data to this article can be found online at https://doi.org/10.1016/j.ces.2023.119578.

References

Alves, M., Grignard, B., Gennen, S., Detrembleur, C., Jerome, C., Tassaing, T., 2015. Organocatalytic synthesis of bio-based cyclic carbonates from CO_2 and vegetable oils. RSC Adv. 5, 53629–53636. https://doi.org/10.1039/C5RA10190E.

Bähr, M., Mülhaupt, R., 2012. Linseed and soybean oil-based polyurethanes prepared via the non-isocyanate route and catalytic carbon dioxide conversion. Green Chem. 14, 483. https://doi.org/10.1039/c2gc16230j.

Cai, X., Matos, M., Leveneur, S., 2019. Structure–Reactivity: Comparison between the carbonation of epoxidized vegetable oils and the corresponding epoxidized fatty acid methyl ester. Ind. Eng. Chem. Res. 58, 1548–1560. https://doi.org/10.1021/acs.iecr.8b05510.

Calabrese, C., Giacalone, F., Aprile, C., 2019. Hybrid catalysts for CO_2 Conversion into cyclic carbonates. Catalysts 9, 325. https://doi.org/10.3390/catal9040325.

Comerford, J.W., Ingram, I.D.V., North, M., Wu, X., 2015. Sustainable metal-based catalysts for the synthesis of cyclic carbonates containing five-membered ring. Green Chem. 17, 1966–1987. https://doi.org/10.1039/C4GC01719F.

Decortes, A., Belmonte, M.M., Benet-Buchholz, J., Kleij, A.W., 2010. Efficient carbonate synthesis under mild conditions through cycloaddition of carbon dioxide to oxiranes using a Zn(salphen) catalyst. Chem. Commun. 46, 4580–4582. https://doi.org/10.1039/C000493F.

Fogg, P.C.T., Gerrard, W., 1991. Solubility of Gases in Liquids. Wiley, Chichester.

Freites Aguilera, A., Rahkila, J., Hemming, J., Nurmi, M., Torres, G., Razat, T., Tolvanen, P., Eränen, K., Leveneur, S., Salmi, T., 2020. Epoxidation of tall oil catalyzed by an ion exchange resin under conventional heating and microwave irradiation. Ind. Eng. Chem. Res. 59, 10397–10406. https://doi.org/10.1021/acs.iecr.0c01288.

Guzmán Agudelo, A.F., Pérez-Sena, W.Y., Kebir, N., Salmi, T., Ríos, L.A., Leveneur, S., 2020. Influence of steric effects on the kinetics of cyclic-carbonate vegetable oils aminolysis. Chem. Eng. Sci. 228, 115954 https://doi.org/10.1016/j.ces.2020.115954.

Haario, H., 2014. ModEst – User s Guide. Profmath Oy, Helsinki.

Haario, H., Saksman, E., Tamminen, J., 2001. An adaptive Metropolis algorithm. Bernoulli 223–242. https://doi.org/10.2307/3318737.

Honda, M., Tamura, M., Nakao, K., Suzuki, K., Nakagawa, Y., Tomishige, K., 2014. Direct cyclic carbonate synthesis from CO_2 and diol over carboxylation/hydration cascade catalyst of CeO_2 with 2-cyanopyridine. ACS Catal. 4, 1893–1896. https://doi.org/10.1021/cs500301d.

Hu, L., Yan, Z., Mo, X., Peng, X., Chen, L., 2020. Hierarchical Co/ZIF-8 as an efficient catalyst for cycloaddition of CO_2 and epoxide. Microporous Mesoporous Mater. 294, 109917 https://doi.org/10.1016/j.micromeso.2019.109917.

Huang, Z., Li, F., Chen, B., Yuan, G., 2016. Cycloaddition of CO_2 and epoxide catalyzed by amino- and hydroxyl-rich graphitic carbon nitride. Cat. Sci. Technol. 6, 2942–2948. https://doi.org/10.1039/C5CY01805F.

Jay, R.R., 1964. Direct titration of epoxy compounds and aziridines. Anal. Chem. 36, 667–668. https://doi.org/10.1021/ac60209a037.

Kohrt, C., Werner, T., 2015. Recyclable bifunctional polystyrene and silica gel-supported organocatalyst for the Coupling of CO_2 with epoxides. ChemSusChem 8, 2031–2034. https://doi.org/10.1002/cssc.201500128.

Kreye, O., Mutlu, H., Meier, M.A.R., 2013. Sustainable routes to polyurethane precursors. Green Chem. 15, 1431–1455. https://doi.org/10.1039/C3GC40440D.

Liang, H., Wang, J., Wang, F., Feng, Y., Kang, M., Wang, Z., 2018. An efficient heterogeneous LiBr/γ-Al_2 $_O$3 catalyst for the cycloaddition of C_O2 with diglycidyl ethers: An efficient heterogeneous LiBr/γ-A_l2_O3 catalyst for the cycloaddition of C_O2 with diglycidyl ethers. J. Chem. Technol. Biotechnol. 93 (8), 2271–2280. https://doi.org/10.1002/jctb.5570.

Liu, M., Liu, B., Liang, L., Wang, F., Shi, L., Sun, J., 2016. Design of bifunctional NH3I-Zn/SBA-15 single-component heterogeneous catalyst for chemical fixation of carbon dioxide to cyclic carbonates. Journal of Molecular Catalysis a: Chemistry 418–419, 78–85. https://doi.org/10.1016/j.molcata.2016.03.037.

Longwitz, L., Steinbauer, J., Spannenberg, A., Werner, T., 2018. Calcium-based catalytic system for the synthesis of bio-derived cyclic carbonates under mild conditions. ACS Catal. 8, 665–672. https://doi.org/10.1021/acscatal.7b03367.

Lu, X.-B., Darensbourg, D.J., 2012. Cobalt catalysts for the coupling of CO_2 and epoxides to provide polycarbonates and cyclic carbonates. Chem. Soc. Rev. 41, 1462–1484. https://doi.org/10.1039/C1CS15142H.

Luo, R., Zhou, X., Zhang, W., Liang, Z., Jiang, J., Ji, H., 2014. New bi-functional zinc catalysts based on robust and easy-to-handle N-chelating ligands for the synthesis of cyclic carbonates from epoxides and CO_2 under mild conditions. Green Chem. 16, 4179–4189. https://doi.org/10.1039/C4GC00671B.

National Center for Biotechnology Information, 2023. PubChem Compound Summary for CID 6371, Phosgene. Retrieved November 17, 2023 from. https://pubchem.ncbi.nlm.nih.gov/compound/Phosgene.

North, M., Pasquale, R., Young, C., 2010. Synthesis of cyclic carbonates from epoxides and CO_2. Green Chem. 12, 1514. https://doi.org/10.1039/c0gc00065e.

Pena Carrodeguas, L., Cristòfol, À., Fraile, J.M., Mayoral, J.A., Dorado, V., Herrerías, C.I., Kleij, A.W., 2017. Fatty acid based biocarbonates: Al-mediated stereoselective preparation of mono-, di- and tricarbonates under mild and solvent-less conditions. Green Chem. 19, 3535–3541. https://doi.org/10.1039/C7GC01206C.

Perez Sena, W.Y., Eränen, K., Kumar, N., Estel, L., Leveneur, S., Salmi, T., 2022. New insights into the cocatalyst-free carbonation of vegetable oil derivatives using heterogeneous catalysts. *J. CO_2 Util.* 57, 101879 https://doi.org/10.1016/j.jcou.2021.101879.

Pérez-Sena, W.Y., Wärnå, J., Eränen, K., Tolvanen, P., Estel, L., Leveneur, S., Salmi, T., 2021. Use of semibatch reactor technology for the investigation of reaction mechanism and kinetics: Heterogeneously catalyzed epoxidation of fatty acid esters. Chem. Eng. Sci. 230, 116206 https://doi.org/10.1016/j.ces.2020.116206.

Petrović, Z.S., 2008. Polyurethanes from vegetable oils. Polym. Rev. 48, 109–155. https://doi.org/10.1080/15583720701834224.

Reid, R.C., Prausnitz, J.M., Poling, B.E., 1988. The Properties of Gases and Liquids, 4th ed. McGraw Hill, New York.

Ruiz, L., Aghmiz, A., Masdeu-Bultó, A.M., Lligados, G., Rondu, J.C., Galia, M., Cádiz, V., 2017. Upgrading castor oil: From heptanal to non-isocyanate poly(amide-hydroxyurethane)s. Polymer 124, 226–234. https://doi.org/10.1016/j.polymer.2017.07.070.

Salmi, T., Mikkola, J.-P., Wärnå, J., 2019. Chemical Reaction Engineering and Reactor Technology, 2nd Edition, CRC Press. Taylor & Francis Group, Boca Raton Florida.

Sankar, M., Ajithkumar, T.G., Sankar, G., Manikandan, P., 2015. Supported imidazole as heterogeneous catalyst for the synthesis of cyclic carbonates from epoxides and CO_2. Catal. Commun. 59, 201–205. https://doi.org/10.1016/j.catcom.2014.10.026.

Saptal, V.B., Bhanage, B.M., 2017. Current advances in heterogeneous catalysts for the synthesis of cyclic carbonates from carbon dioxide. Curr. Opin. Green Sustain. Chem. 3, 1–10. https://doi.org/10.1016/j.cogsc.2016.10.006.

Su, Q., Sun, J., Wang, J., Yang, Z., Cheng, W., Zhang, S., 2014. Urea-derived graphitic carbon nitride as an efficient heterogeneous catalyst for CO_2 conversion into cyclic carbonates. Cat. Sci. Technol. 4, 1556. https://doi.org/10.1039/c3cy00921a.

Vanags, E., Abolins, A., Cabulis, U., 2023. Lipase catalyzed self-epoxidation of tall oil fatty acids in batch and continuous flow conditions. J. Polym. Environ. 31, 2166–2176. https://doi.org/10.1007/s10924-023-02783-4.

Webster, D.C., 2003. Cyclic carbonate functional polymers and their applications. Prog. Org. Coat. 47, 77–86. https://doi.org/10.1016/S0300-9440(03)00074-2.

Wikström, W., Freites Aguilera, A., Tolvanen, P., Lassfolk, R., Medina, A., Eränen, K., Salmi, T., 2023. Fatty acid epoxidation on enzymes: experimental study and modelling of batch and semibatch operation. Ind. Eng. Chem. Res. 62, 9169–9187. https://doi.org/10.1021/acs.iecr.3c00890.

Zhang, W.-H., He, P.-P., Wu, S., Xu, J., Li, Y., Zhang, G., Wei, X.-Y., 2016. Graphene oxide grafted hydroxyl-functionalized ionic liquid: A highly efficient catalyst for cycloaddition of CO_2 with epoxides. Appl. Catal. A 509, 111–117. https://doi.org/10.1016/j.apcata.2015.10.038.

Zhao, L., Liu, N., Huang, H., Wang, X., Huang, X., 2019. Synthesis of propylene carbonate from carbon dioxide through high activity of magnesium oxide. J. Chem. Eng. Jpn 52, 406–412. https://doi.org/10.1252/jcej.18we073.